Electromagnetic density of states and absorption of radiation by aggregates of nanospheres with multipole interactions

Vadim A. Markel*
Department of Radiology, University of Pennsylvania, Philadelphia, Pennsylvania 19104, USA

Vitaliy N. Pustovit†
Department of Physics, Jackson State University, Jackson, Mississippi 39217, USA

Sergei V. Karpov‡
L.V. Kirensky Institute of Physics, Russian Academy of Sciences, Siberian Branch, Krasnoyarsk 660036, Russia

Alexander V. Obuschenko
Moscow Institute of Physics and Technology, Dolgoprudny, Moscow Region 141700, Russia

Valeriy S. Gerasimov and Ivan L. Isaev
Department of Physics and Engineering, Krasnoyarsk State Technical University, Krasnoyarsk 660028, Russia
(Received 15 December 2003; revised manuscript received 9 April 2004; published 27 August 2004)

We calculate the quasistatic electromagnetic density of states for aggregates of touching spheres, in particular, linear chains and computer-generated random fractal aggregates. Multipole moments with orders of up to $L=64$ are taken into account for random aggregates with the number of particles of up to $N=100$ and up to $L=8000$ for linear chains. Extensive comparisons with the dipole approximation and geometrical cluster renormalization method are performed. Extinction spectra are calculated for several metals and black carbon. Long wavelength electromagnetic properties of fractal aggregates are considered in details.

DOI: 10.1103/PhysRevB.70.054202 PACS number(s): 78.67.Bf, 41.20.Cv, 73.20.Mf

I. INTRODUCTION

The optical properties of fractal nanoaggregates continue to attract significant attention.[1–11] These objects were demonstrated to exhibit an unusual type of inhomogeneous spectral broadening which, in turn, leads to a variety of interesting physical phenomena such as strong fluctuations of local fields and enhancement of nonlinear optical responses,[12–17] nanometer-scale photomodification, and burning of polarization-selective spectral holes.[18–24] The nature of localization of electromagnetic modes in fractal aggregates have been a subject of intensive study.[16,25–30] Optical properties of fractal soot are of significant importance in atmospheric optics and climate research.[31–34] Another topic of recent interest is femtosecond dynamics of local excitations in fractal aggregates.[35]

The physical model of a fractal aggregate almost exclusively used in the literature is that of an array of small spherical particles of the same size which form a rigid self-supporting aggregate. To be more specific, the particles are allowed to touch at a mathematical point, and two touching particles are assumed to be rigidly connected to each other. An aggregate is said to be self-supporting if every particle is connected to at least one other particle. The set of coordinates specifying the location of the center of each spherical particle completely defines an aggregate. These coordinates are usually obtained by simulating an aggregation process on a computer. Aggregates generated in this manner are random. The fractal dimension, D, can be found by studying statistical characteristics of an ensemble of such aggregates. In particular, the pair density-density correlation function $p(r)$ is defined as the probability density to find a pair of distinct particles belonging to the same aggregate separated by the distance r. It has the intermediate asymptote $p(r)\approx r^{D-1}/N$, $a\ll r\ll R_g$, where a is the radius of a single particle and R_g is the average gyration radius of the aggregate. Another way of obtaining D is by studying the dependence of R_g on the number of particles in the aggregate, N. One expects that if $p(r)$ is described by the above asymptote, $R_g\propto N^{1/D}$.

The optical properties of fractal aggregates have long been studied in the dipole approximation (DA) (see, for example, Refs. 9, 36, and 37). In this approximation, each particle is replaced by an elementary dipole $\boldsymbol{d}_i \exp(-i\omega t)$ located at its center, where the index i labels particles in an aggregate. By considering the interaction of the dipoles with each other and the incident field, one can obtain a self-consistent system of linear equations coupling the amplitudes $\boldsymbol{d}_i$ to each other and to the external field. All electromagnetic and, consequently, optical properties of an aggregate within the DA can be expressed in terms of $\boldsymbol{d}_i$.

The DA allows one to understand many of the optical phenomena listed earlier *in principle*. Most importantly, it captures the main feature of the optical properties of fractals, which is the inhomogeneous broadening of the absorption spectrum, with each homogeneous spectral line corresponding to a certain electromagnetic eigenmode of the system. However, the DA is inaccurate for touching spheres. This fact was recognized fairly early[38] and has a simple physical explanation. Indeed, even when the incident field is almost homogeneous over the volume of a given particle (or even

the whole aggregate, as is assumed in the quasistatic limit), the secondary fields scattered by neighboring particles are highly inhomogeneous. These inhomogeneous fields excite higher multipole moments inside the particles, which are not accounted for in the DA. For example, the DA predicts that the long wavelength tail of absorption spectrum of silver colloid aggregates terminates at approximately 500 nm, while experimentally it is known to extend well into the infrared (IR) spectral region.[2,8,10,11,39]

Independently of the research aimed specifically at the optics of fractal aggregates, rigorous numerical methods have been developed for solving the electromagnetic boundary problem for several interacting spheres by Gerardy and Ausloos,[40] Claro,[41–46] Mackowski,[47–50] and others. These methods allow one to overcome the limitations of the DA and to take into account excitation of higher multipole moments inside each sphere. The main disadvantage of this approach is large computational complexity. The rigorous consideration of boundary conditions on the surface of each sphere results in an infinite-dimensional system of equations. To be solved on a computer, the system must be truncated at a finite multipole order L which leads to $NL(L+2)$ linear equations. The minimum value of L required for convergence, $L_{\min}$, depends on the dielectric function of the scattering material $\epsilon(\omega)$, and on the distance between the spheres. The problem becomes especially complicated when the spheres are touching. In this case, it has been demonstrated that $L_{\min}$ becomes very large when $\epsilon(\omega)$ is large.[47,51,52] At the same time, perturbative[53] or mean-field[36] approaches lead to inaccurate results in this case due to strong resonant electromagnetic interaction.[51]

The coefficients in the system of equation discussed in the previous paragraph depend on the wavelength due to dispersion of the dielectric function $\epsilon(\omega)$. The standard approach adopted in the literature is to solve this system each time for a new value of the wavelength (or a different material). This makes the computations even more time consuming when optical spectra rather than optical characteristics at a given wavelength must be calculated. This should be contrasted with the spectral approach developed in Refs. 54 and 55 and later, in the DA and with specific application to fractal aggregates, in Ref. 37. (It should be noted that at the time when these papers were published, the existing computer technology did not allow one to perform simulations for random aggregates with the number of particles and the maximum order of multipoles included significantly larger than one.) The approach adopted in Ref. 37 is based on diagonalization of a wavelength-independent interaction matrix. Thus, the computationally intensive part is carried out only once for a given aggregate geometry. After this is done, optical cross sections of the aggregate for arbitrary wavelength or arbitrary material can be calculated very efficiently by simple summation.

The mathematical formalism of Ref. 37 was developed using two approximations. The first one is the quasistatic approximation. This approximation is crucial since beyond the quasistatic limit the interaction operator becomes non-Hermitian and, even more importantly, wavelength dependent. The second approximation is the DA which allows one to reduce the number of equations. However, the interaction operator remains Hermitian and wavelength independent even beyond the DA. Therefore, as long as we remain in the framework of the quasistatics, the approach of Ref. 37 can be generalized to include higher multipolar interactions, which is done in this paper. We have developed a computationally efficient algorithm for including high-order multipolar moments. Using this approach we have calculated the electromagnetic density of states and extinction cross sections for linear chains of touching spheres and for computer-generated random fractal aggregates. We have shown that exact account of higher multipolar interactions allows one to describe certain spectral features which are not seen in the dipole approximation or when relatively low orders of multipole moments are used. In particular, anomalously high collective absorption at the plasmon resonance frequency of an isolated sphere is one of these features. We show that it takes place due to short-range pair interactions.

In the first part of the paper we focus on the electromagnetic density of states (DOS). Although such characteristics as absorption spectra and spatial distribution of local fields are more relevant physically and can be directly compared with experimental data, the description based on the DOS is more general since it depends only on the shape of the scatterer but not on the wavelength or the material. The form of the DOS provides an important insight into the nature of interaction of a scatterer with external electromagnetic field. In particular, it allows one to predict, at least qualitatively, the spectral region in which strong resonance interaction and a number of physical phenomena that are associated with it can be expected. In the second part of the paper absorption spectra of several materials are calculated.

The paper is organized as follows. In Sec. II we briefly review the mathematical formalism of the electromagnetic DOS in the context of the quasistatic scattering problem. We also discuss in this section some general properties of DOS which follow from simple physical considerations and are not limited to any particular shape of the scatterer. These properties have important implications for long wavelength tales of extinction spectra. Next, we derive a generalization of an extinction sum rule which was previously reported for ellipsoids and discuss its relation to the properties of DOS. Finally, we obtain matrix elements of the electromagnetic interaction operator in a discrete basis using Maxwell's equations in the integral form.

In Sec. III we describe the numerical methods used to generate random fractal aggregates and to compute the corresponding DOS and extinction spectra. We have used three different kinds of random fractal aggregates in simulations: lattice cluster-cluster aggregates (CCA) with the fractal dimension $D \approx 1.8$ and off-lattice aggregates with fractal dimensions $D \approx 1.3$ and $D \approx 2.3$. Optical properties were calculated using the representation of the DOS as a continued fraction.[56] This is a very efficient iterative numerical method. Similar to the conjugate gradient method, it does not update the interaction matrix during the iterations, but has better convergence properties for the specific problem studied in this paper.

Section IV contains the results of simulations. We start with the simplest case of linear chains of spheres, and proceed with the DOS for random fractal aggregates of different

types. Next, extinction spectra for several scattering materials are calculated. We also compare the obtained results with the DA and with the geometrical cluster renormalization method (GCRM).[57,58] The latter corrects the deficiency of the DA by introducing geometrical intersections of neighboring particles and has played an important role in a number of papers.[2,3,6,10,22,39,59–62] Although the results obtained within the GCRM have been extensively compared with the experimental data, validation of the method by comparison with rigorous simulations has not been done so far.

Finally, Sec. V contains a summary and discussion of obtained results.

II. THEORY

A. Formulation of the eigenproblem

We work in a frequency domain. The electromagnetic frequency is denoted by ω and the corresponding free-space wavelength is $\lambda=2\pi c/\omega$. Let the dielectric function $\epsilon(\boldsymbol{r})$ (with the frequency dependence implied) be given by

$$\epsilon(\boldsymbol{r}) = \begin{cases} \epsilon, & \text{if } \boldsymbol{r} \in V \\ 1, & \text{otherwise} \end{cases}, \tag{1}$$

where V is the region occupied by scattering material (an array of nonintersecting but possibly touching spheres in our case). The volume of the region V will be denoted by v later. Further, we assume that λ is much larger than the characteristic size of the scatterer. Correspondingly, the quasistatic limit is used throughout this paper. In this limit all electromagnetic and, consequently, optical properties can be obtained from the Laplace equation

$$\nabla^2 \epsilon(\boldsymbol{r}) \boldsymbol{E}(\boldsymbol{r}) = 0, \tag{2}$$

where $\boldsymbol{E}$ is the electric field. One can formulate an eigenproblem based on this equation. However, to retain more similarity with the mathematical formalism of Refs. 37 and 63, it is instructive to start instead from the integral equation for the polarization function $\boldsymbol{P}=[(\epsilon-1)/4\pi]\boldsymbol{E}$ which satisfies

$$\boldsymbol{P}(\boldsymbol{r}) = \chi\left[\boldsymbol{E}_0 + \int_V \hat{G}_R(\boldsymbol{r},\boldsymbol{r}')\mathbf{P}(\boldsymbol{r}')d^3r'\right]. \tag{3}$$

Here

$$\chi = \frac{3}{4\pi}\frac{\epsilon-1}{\epsilon+2} \tag{4}$$

is the coupling constant, $\boldsymbol{E}_0$ is the incident field assumed to be constant inside the region V and $\hat{G}_R(\boldsymbol{r},\boldsymbol{r}')$ is the regular part of the dyadic free space Green's function of the Maxwell equations. It is related to the full Green's function $\hat{G}$ (which contains a singular part) by

$$\hat{G}(\boldsymbol{r},\boldsymbol{r}') = \hat{G}_R(\boldsymbol{r},\boldsymbol{r}') - \frac{4\pi}{3}\delta(\boldsymbol{r}-\boldsymbol{r}'), \tag{5}$$

where the components of $\hat{G}$ are given in the quasistatic limit by

$$G_{\alpha\beta}(\boldsymbol{r},\boldsymbol{r}') = -\frac{\partial^2}{\partial r_\alpha \partial r'_\beta}\frac{1}{|\boldsymbol{r}-\boldsymbol{r}'|}. \tag{6}$$

Note that the DA can be obtained from Eq. (3) by assuming that polarization inside each spherical particle is constant.

If V is finite, any physically reasonable polarization function must be square integrable, since the rate of absorption of electromagnetic energy by the object is $\propto\int_V |\boldsymbol{P}|^2 d^3r$. Therefore, $\boldsymbol{P}(\boldsymbol{r})$ is an element of a Hilbert space $\mathcal{H}$.[64] It can be seen that the integral operator on the right-hand side of Eq. (3) maps this space onto itself. We denote this operator by $W:\mathcal{H}\to\mathcal{H}$. We also introduce abstract vectors $|P\rangle$ and $|E_0\rangle$ which correspond to $\boldsymbol{P}(\boldsymbol{r})$ and $\boldsymbol{E}_0$, respectively, and rewrite Eq. (3) in operator notation as

$$|P\rangle = \chi[|E_0\rangle + W|P\rangle]. \tag{7}$$

The formal solution to Eq. (7) can be expressed through the resolvent of the operator W, $R(z;W)\equiv(z-W)^{-1}$:

$$|P\rangle = (z-W)^{-1}|E_0\rangle = R(z;W)|E_0\rangle. \tag{8}$$

All physical quantities of interest can be obtained from the matrix elements of the resolvent. In particular, the extinction cross section is given by

$$\sigma_e = \frac{4\pi k}{|\boldsymbol{E}_0|^2}\mathrm{Im}\int_V \boldsymbol{E}_0^*\cdot\boldsymbol{P}(\boldsymbol{r})d^3r = \frac{4\pi k}{|E_0|^2}\mathrm{Im}\,\langle E_0|P\rangle$$
$$= \frac{4\pi k}{|\mathbf{E}_0|^2}\mathrm{Im}\,\langle E_0|R(z;W)|E_0\rangle. \tag{9}$$

Thus, σ_e is proportional to the diagonal matrix element of the resolvent.

Since we are working in the quasistatic limit, both operators W and R are Hermitian and have the same set of eigenvectors. Let us denote the eigenvalues and eigenvectors of W by w_n and $|n\rangle$, so that $W|n\rangle=w_n|n\rangle$. Then we can rewrite Eq. (9) as

$$\sigma_e = \frac{4\pi k}{|\boldsymbol{E}_0|^2}\mathrm{Im}\sum_n \frac{\langle E_0|n\rangle\langle n|E_0\rangle}{z-w_n}. \tag{10}$$

B. Density of states

Let us also define the weighted DOS $\Gamma(w)$ according to

$$\Gamma(w) = \sum_n \frac{\langle E_0|n\rangle\langle n|E_0\rangle}{v|\boldsymbol{E}_0|^2}\delta(w-w_n). \tag{11}$$

Since $\langle E_0|E_0\rangle=|\boldsymbol{E}_0|^2 v$, DOS is normalized: $\int\Gamma(w)dw=1$. Using the earlier definition of Γ, (10) can be equivalently rewritten as

$$\sigma_e = 4\pi k v\ \mathrm{Im}\int\frac{\Gamma(w)dw}{z-w}. \tag{12}$$

If we introduce real and imaginary parts of the variable z according to[65]

$$z = X - i\delta, \tag{13}$$

we also have

$$\sigma_e = 4\pi k v\,\delta \int \frac{\Gamma(w)dw}{(X-w)^2+\delta^2}. \tag{14}$$

Thus, in the limit of weak absorption ($\delta \to 0$), we have

$$\sigma_e = 4\pi^2 k v \Gamma(X). \tag{15}$$

On the other hand, the earlier equation can be viewed as an alternative definition of the DOS:

$$\Gamma(w) = \frac{1}{\pi v |\boldsymbol{E}_0|^2} \lim_{\delta \to 0} \mathrm{Im}\langle E_0 | R(w - i\delta; W) | E_0 \rangle. \tag{16}$$

The advantage of the description based on DOS is that the latter is independent of the material properties of the scatterer and depends only on its shape. Thus, calculation of DOS can give important insights about the influence of geometry on the optical properties. It is important to note that any numerical calculations based on formula (11) will produce an essentially singular DOS, while the true spectrum of the infinite-dimensional operator W may be continuous. This problem can be solved by appropriate smoothing, i.e., by replacing the delta functions in Eq. (11) by Lorentzians of finite width. A mathematically equivalent, and a more practical approach is to use the definition (16) with a small but finite (and constant) value of δ. The numerical results obtained in this manner are adequate as long as the value of constant δ used in Eq. (16) is smaller than the actual value of $\delta = -\mathrm{Im}(z)$ for the scattering material. Therefore, calculation of scattering properties high-conductivity metals pose, in general, a very serious computational challenge, since the value of δ can be very small for such metals, especially in the IR and far-IR spectral regions.

C. General properties of the DOS

Here we consider some limitations on the form of DOS which follow from general physical considerations. Namely, we will discuss an analogy between eigenvalues w and depolarization factors ν of ellipsoids and certain consequences of an exact sum rule for the extinction cross section which follows from casualty.

1. Generalized depolarization factors

By using the identity

$$z = \frac{4\pi}{3}\frac{\epsilon+2}{\epsilon-1} = \frac{4\pi}{3} + \frac{4\pi}{\epsilon-1}, \tag{17}$$

Eq. (12) can be rewritten as

$$\sigma_{\mathrm{e}} = k v\ \mathrm{Im} \int \frac{\Gamma(w)dw}{1/(\epsilon-1) + (1/3 - w/4\pi)}. \tag{18}$$

Compare this expression to the well-known formula for ellipsoids in the quasistatic limit. For the external field aligned with one of the major axis of the spheroid (labeled by $p = 1,2,3$), this formula reads[66]

$$\sigma_{\mathrm{e}}^{(p)} = k v\ \mathrm{Im} \frac{1}{1/(\epsilon-1) + \nu^{(p)}}. \tag{19}$$

By analogy, we can introduce generalized depolarization factors for a scatterer of an arbitrary shape, according to $\nu_n = 1/3 - w_n/4\pi$, where w_n's are the eigenvalues of the corresponding operator W. We expect that the generalized depolarization factors satisfy the same inequality as in the case of ellipsoids, namely $0 < \nu_n < 1$. Correspondingly, we come to the conclusion that $-8\pi/3 < w_n < 4\pi/3$ and $\Gamma(w)$ turns to zero unless $w \in (-8\pi/3, 4\pi/3)$.

Although a rigorous mathematical proof of the earlier property of $\Gamma(w)$ is not readily available, the physical interpretation is quite obvious. Consider an electromagnetic resonance in a body of a given shape that takes place when $\mathrm{Re}[1/(\epsilon-1) + \nu_n] = 0$. The resonance condition can be written as $\mathrm{Re}(\epsilon) = 1 - 1/\nu_n$. First, we prove that ν_n cannot be negative. Indeed, if $\nu_n < 0$, the resonance takes place for $\mathrm{Re}(\epsilon) > 1$. Therefore, we can imagine a hypothetical dielectric of the same shape and with purely real electrostatic permeability $\epsilon(\omega = 0) = 1 - 1/\nu_n > 1$. Since this is the resonance value of ϵ and the operator W does not depend on frequency, the dielectric can be polarized so that the polarization function coincides (up to an arbitrary multiplicative constant) with the nth resonant mode. Such polarization will be equivalent to a stable distribution of charges inside the dielectric which can exist indefinitely without external field. But this is known to be impossible. Thus, ν_n can not be negative. The proof that ν_n cannot be larger than unity is similar, but the hypothetical dielectric is replaced by a void of the same shape in an infinite medium with $\epsilon = 1/(1 - 1/\nu_n)$.

2. Sum rule for extinction and the long wavelength behavior

Let the incident field be linearly polarized along the z axis. Then, as is shown in the Appendix, the extinction cross section of an arbitrary scatterer satisfies the following sum rule

$$\int_0^\infty \sigma_{\mathrm{e}}(\lambda) d\lambda = 4\pi^3 \alpha_{zz}, \tag{20}$$

where $\hat{\alpha}$ is the electrostatic polarizability tensor of the scattering particle. Note that Eq. (20) is extremely general. It is not limited to the quasistatic approximation, as the integration in Eq. (20) is over all values of λ, and also holds for scatterers of arbitrary size and shape, with possibly spatially inhomogeneous, tensorial, and nonlocal dielectric function.

One important conclusion about the DOS can be inferred from the earlier sum rule. Since the electrostatic polarizability of any finite object is also finite, integral (20) must converge. This puts some restrictions on the asymptotic behavior of $\sigma_{\mathrm{e}}(\lambda)$. In particular, for $\lambda \to \infty$, σ_{e} must approach zero faster than $1/\lambda$. We will show that the property of the DOS

discussed in Sec. II C 1 is consistent with this fact using the following two examples. First consider dielectric material with ϵ given by

$$\epsilon(\omega) = 1 - \sum_k \frac{f_k^2}{\omega^2 - \omega_k^2 + i\omega\gamma_k}. \tag{21}$$

Using this expression, we obtain in the limit $\omega \to 0$:

$$X(\omega) = X_0 = \frac{4\pi}{3} + \frac{4\pi}{S_1}, \quad \delta(\omega) = \frac{4\pi S_2}{S_1^2}\omega \quad (\omega \to 0), \tag{22}$$

where $S_1 = \Sigma_k\, (f_k/\omega_k)^2$, $S_2 = \Sigma_k\, f_k^2\gamma_k/\omega_k^4$ and X and δ are defined by Eq. (13). It can be seen that for dielectrics the long wavelength limit of the variable $X(\omega)$ lies outside of the "absorption band" $(-8\pi/3, 4\pi/3)$. Therefore, using Eq. (14), we obtain the following asymptotic expression for σ_e in the long wavelength limit:

$$\sigma_e(\omega) = Av\omega^2, \quad A = \frac{(4\pi)^2 S_2}{cS_1^2}\int_{-8\pi/3}^{4\pi/3} \frac{\Gamma(w)dw}{(X_0 - w)^2} \quad (\omega \to 0). \tag{23}$$

Thus, for dielectrics we obtain a universal scaling $\sigma_e \propto \omega^2 \propto 1/\lambda^2$ when $\lambda \to \infty$ with a coefficient depending on the material properties and the scatterer shape.

A more complicated situation is encountered for conductors. At sufficiently low frequency any conductor can be described by the dielectric function of the form

$$\epsilon(\omega) = 1 - \frac{\omega_p^2}{\omega(\omega + i\gamma)}, \tag{24}$$

so that the asymptotic expressions for $X(\omega)$ and $\delta(\omega)$ are

$$X(\omega) = \frac{4\pi}{3} - \frac{4\pi\omega^2}{\omega_p^2}, \quad \delta(\omega) = \frac{4\pi\gamma\omega}{\omega_p^2} \quad (\omega \to 0). \tag{25}$$

Thus, the value of $X(\omega)$ stays inside the absorption band and approaches its right bound when $\omega \to 0$. As a result, the long wavelength extinction cross section of metal particles can be very sensitive to the exact form of the DOS near the point $w = 4\pi/3$. In particular, if we assume that $\Gamma(w) = (4\pi/3 - w)^\alpha$ if $w < 4\pi/3$, and γ is sufficiently small so that we can replace Lorentzians by delta function in integral (14), we obtain the asymptote

$$\sigma_e(\omega) = Av\omega^{1+2\alpha}, \quad A = \frac{\pi(4\pi)^{1+\alpha}}{c\omega_p^{2\alpha}} \quad (\omega \to 0). \tag{26}$$

Unlike in the case of dielectrics, the scaling exponent is not independent of the form of DOS. Note that the extinction sum rule (20) is satisfied for any $\alpha > 0$. Note also that the extinction cross section can experience a cross over from the $1/\lambda$ decay to $1/\lambda^{1+2\alpha}$ when the variable X approaches its right bound and crosses over into the interval where the scaling asymptote of $\Gamma(w)$ is valid.

D. Matrix representation of the operator *W*

Consider N spherical particles with centers at $\boldsymbol{r}_i$ $(i = 1, \ldots, N)$ and radius a. The theory can be easily modified for polydisperse spheres as well. In order to calculate the DOS and the extinction cross section, we must obtain a matrix representation of the operator W. Therefore, we start with constructing a discrete basis in the Hilbert space $\mathcal{H}$. Consider the following scalar functions:

$$\psi_{lm}^{(1)}(\boldsymbol{r}) = \begin{cases} (r/a)^l Y_{lm}(\hat{\boldsymbol{r}}), & r \leqslant a \\ 0, & r > a, \end{cases} \tag{27}$$

$$\psi_{lm}^{(2)}(\boldsymbol{r}) = \begin{cases} (a/r)^{l+1} Y_{lm}(\hat{\boldsymbol{r}}), & r \geqslant a \\ 0, & r < a, \end{cases} \tag{28}$$

and corresponding (electrostatic) vector spherical harmonics

$$\boldsymbol{X}_{ilm}^{(1)}(\boldsymbol{r}) = (la)^{-1/2}\, \nabla\, \psi_{lm}^{(1)}(\boldsymbol{r} - \boldsymbol{r}_i), \tag{29}$$

$$\mathbf{X}_{ilm}^{(2)}(\boldsymbol{r}) = [(l+1)a]^{-1/2}\, \nabla\, \psi_{lm}^{(2)}(\boldsymbol{r} - \boldsymbol{r}_i). \tag{30}$$

Here $Y_{lm}(\hat{\boldsymbol{x}})$ is a spherical function defined by the polar angles of the unit vector $\hat{\boldsymbol{x}}$ in the laboratory frame. The factors $(la)^{-1/2}$ and $[(l+1)a]^{-1/2}$ are introduced for normalization. It can be verified that

$$\int_V \boldsymbol{X}_{ilm}^{(1)*}(\boldsymbol{r}) \cdot \boldsymbol{X}_{i'l'm'}^{(1)}(\boldsymbol{r}) d^3r = \delta_{ii'}\delta_{ll'}\delta_{mm'}. \tag{31}$$

Here integration is taken over the whole space occupied by the scattering material (collection of spheres). It follows from Eq. (31) that functions $\boldsymbol{X}_{ilm}^{(1)}(\boldsymbol{r})$ constitute an orthonormal basis in $\mathcal{H}$ (the proof of completeness is straightforward). We also have

$$\int_{|\boldsymbol{r}' - \boldsymbol{r}_i| \leqslant a} \hat{G}_R(\boldsymbol{r}, \boldsymbol{r}') \boldsymbol{X}_{ilm}^{(1)}(\boldsymbol{r}') d^3r' = -\frac{4\pi(l-1)}{3(2l+1)} \boldsymbol{X}_{ilm}^{(1)}(\boldsymbol{r}),$$

$$\text{if } |\boldsymbol{r} - \boldsymbol{r}_i| < a, \tag{32}$$

$$\int_{|\boldsymbol{r}' - \boldsymbol{r}_i| \leqslant a} \hat{G}_R(\boldsymbol{r}, \boldsymbol{r}') \boldsymbol{X}_{ilm}^{(1)}(\boldsymbol{r}') d^3r' = -\frac{4\pi\sqrt{l(l+1)}}{2l+1} \boldsymbol{X}_{ilm}^{(2)}(\boldsymbol{r}),$$

$$\text{if } \quad |\boldsymbol{r} - \boldsymbol{r}_i| > a, \tag{33}$$

$$\int_{|\boldsymbol{r}' - \boldsymbol{r}_i| > a} \hat{G}_R(\boldsymbol{r}, \boldsymbol{r}') X_{ilm}^{(2)}(\boldsymbol{r}') d^3\boldsymbol{r}' = -\frac{4\pi\sqrt{l(l+1)}}{2l+1} \boldsymbol{X}_{ilm}^{(1)}(\boldsymbol{r}),$$

$$\text{if } |\boldsymbol{r} - \boldsymbol{r}_i| < a, \tag{34}$$

$$\int_{|\boldsymbol{r}' - \boldsymbol{r}_i| > a} \hat{G}_R(\boldsymbol{r}, \boldsymbol{r}') \boldsymbol{X}_{ilm}^{(2)}(\boldsymbol{r}') d^3r' = -\frac{4\pi(l+2)}{3(2l+1)} \boldsymbol{X}_{ilm}^{(2)}(\boldsymbol{r}),$$

$$\text{if } |\boldsymbol{r} - \boldsymbol{r}_i| > a. \tag{35}$$

Here in Eqs. (32) and (33) the integrals are taken over the volume of *i*th sphere while integrals ((34)) and ((35)) are taken over the supplement of the volume of *i*th sphere to the whole space.

Let us denote abstract vectors in Hilbert space $\mathcal{H}$ that correspond to $\boldsymbol{X}_{ilm}^{(1)}$ as $|ilm\rangle$. Now, using the relations (32)–(33) we can obtain the matrix element of the linear operator W:

$$\langle ilm|W|i'l'm'\rangle = -\frac{4\pi}{3}\frac{l-1}{2l+1}\delta_{ii'}\delta_{ll'}\delta_{mm'} + M_{ilm}^{i'l'm'}(1-\delta_{ii'}), \tag{36}$$

where

$$M_{ilm}^{i'l'm'} = \int_{|\boldsymbol{r}-\boldsymbol{r}_i|<a} d^3r \int_{|\boldsymbol{r}'-\boldsymbol{r}_{i'}|<a} d^3r' \boldsymbol{X}_{ilm}^{(1)*}(\boldsymbol{r})\cdot\hat{G}_{\mathrm{R}}(\boldsymbol{r},\boldsymbol{r}')\boldsymbol{X}_{i'l'm'}^{(1)}(\boldsymbol{r}') \quad (i\neq i'). \tag{37}$$

Using Eq. (33), we obtain

$$M_{ilm}^{i'l'm'} = -\frac{4\pi\sqrt{l'(l'+1)}}{2l'+1} \times \int_{|\boldsymbol{r}-\boldsymbol{r}_i|<a} \boldsymbol{X}_{ilm}^{(1)*}(\boldsymbol{r})\cdot\boldsymbol{X}_{i'l'm'}^{(2)}(\boldsymbol{r})d^3r \quad (i\neq i'). \tag{38}$$

The earlier integral can be calculated with the use of the formulas for translation of solid spherical harmonics[67]

$$\psi_{lm}^{(2)}(\boldsymbol{r}+\Delta\boldsymbol{r}) = \sum_{l'm'} K_{lm}^{l'm'}(\Delta\boldsymbol{r})\psi_{l'm'}^{(1)}(\boldsymbol{r}) \quad (\Delta r > r), \tag{39}$$

where

$$K_{lm}^{l'm'}(\Delta\mathbf{r}) = \frac{(-1)^{l'+m'}}{2l'+1}\sqrt{\frac{4\pi(2l+1)(2l'+1)(l+l'+m-m')!\,(l+l'-m+m')!}{[2(l+l')+1](l-m)!\,(l+m)!\,(l'-m')!\,(l'+m')!}}\psi_{l+l',m'-m}^{(2)}(\Delta\boldsymbol{r}). \tag{40}$$

Now we use the definitions of $\boldsymbol{X}_{ilm}^{(2)}(\boldsymbol{r})$ (30) and the formula (39) to obtain the translation rule for vector spherical harmonics

$$\boldsymbol{X}_{i'l'm'}^{(2)}(\boldsymbol{r}) = \sum_{l''m''}\sqrt{\frac{l''}{l'+1}}K_{l'm'}^{l''m''}(\boldsymbol{r}_{ii'})\boldsymbol{X}_{il''m''}^{(1)}(\boldsymbol{r}), \tag{41}$$

where $\boldsymbol{r}_{ii'}=\boldsymbol{r}_i-\boldsymbol{r}_{i'}$. Substitution of this expansion into integral (38) yields

$$M_{ilm}^{i'l'm'} = -\frac{4\pi\sqrt{ll'}}{2l'+1}K_{l'm'}^{lm}(\boldsymbol{r}_{ii'}) \tag{42}$$

$$= -4\pi(-1)^{l+m}\sqrt{\frac{4\pi ll'(l+l'+m-m')!\,(l+l'-m+m')!}{[2(l+l')+1](2l+1)(2l'+1)(l-m)!\,(l+m)!\,(l'-m')!\,(l'+m')!}}\psi_{l+l',m'-m}^{(2)}(\boldsymbol{r}_{ii'}). \tag{43}$$

This can be also written in terms of the associated Legendre polynomials $P_l^m(x)$ as

$$M_{ilm}^{i'l'm'} = -4\pi(-1)^{l+m}\left(\frac{a}{r_{ii'}}\right)^{l+l'+1}S_{lm}^{l'm'}P_{l+l'}^{m'-m}(\cos\,\theta_{ii'})e^{i(m'-m)\varphi_{ii'}}. \tag{44}$$

Here $\theta_{ii'}$ and $\varphi_{ii'}$ are the polar angles of the vector $\boldsymbol{r}_{ii'}=\boldsymbol{r}_i-\boldsymbol{r}_{i'}$ in the laboratory frame and $S_{lm}^{l'm'}$ is given by

$$S_{lm}^{l'm'} = \frac{\sqrt{ll'}(l+l'+m-m')!}{\sqrt{(2l+1)(2l'+1)(l+m)!\,(l-m)!\,(l'+m')!\,(l'-m')!}}. \tag{45}$$

The expressions (44) and (45), together with Eq. (36) completely define the matrix element $\langle ilm|W|i'l'm'\rangle$. It can be easily verified that the matrix $\langle ilm|W|i'l'm'\rangle$ is Hermitian. It is essentially equivalent to the matrix derived in Ref. 48; the

only difference is that here it was obtained from the integral equations formalism.

The matrix obtained above is infinite. We will truncate it later. The maximum value of l and l' used for this truncation is denoted by L.

In addition to matrix elements of W, we also need an expression for the vector $|E_0\rangle$. Omitting a trivial derivation, we adduce the result

$$|E_0\rangle = \sqrt{\frac{4\pi a^3}{3}} \sum_{i=1}^{N} \left[iE_{0x} \frac{|i11\rangle + |i1-1\rangle}{\sqrt{2}} - E_{0y} \frac{|i11\rangle - |i1-1\rangle}{\sqrt{2}} + E_{0z}|i10\rangle \right]. \quad (46)$$

Here E_{0x}, E_{0y}, and E_{0z} denote the Cartesian components of the polarization vector $\boldsymbol{E}_0$.

Note that the matrix elements of W with $l=l'=1$ correspond to the DA. The corresponding terms decay with distance between two spheres as $1/r_{ii'}^3$ which is characteristic for the dipole coupling. The terms with higher values of l and l' describe interaction of higher multipoles. This interaction is only important for spheres which are close to each other (generally, separated by less that one sphere diameter).

III. NUMERICS

A. Generation of fractal aggregates

We have generated the following three types of fractal aggregates: lattice cluster-cluster aggregates with fractal dimension $D \approx 1.8$ and off-lattice aggregates with fractal dimensions $D \approx 1.3$ and $d \approx 2.3$.

In the case of lattice aggregates, we used the aggregation model introduced by Meakin[68] and Jullien *et al.*[69] Namely, particles were sparsely and randomly distributed on a cubic lattice at the initial moment of time and then allowed to move randomly in all directions, sticking on contact. The subaggregates formed in this process continued to move, colliding and sticking with other subaggregates and isolated monomers, until agglomerates of desired size were formed.

The off-lattice aggregates were generated using a new algorithm intended for simulation of aggregation kinetics in sols. A simplified version of such generator was first used in Ref. 2 to study optical absorption by fractal-structured Ag sols. The main purpose of the proposed algorithm is to simulate aggregates of touching spheres with geometrical structure resembling that of real colloid aggregates in sols as close as possible.

First, it is clear that in order to achieve a high level of such resemblance, the aggregation process should be off-lattice. Indeed, the growth of real aggregates is the result of random Brownian motion of individual particles and aggregates which is not restricted to any spatial directions or lattices. Second, an important factor affecting the geometrical structure of the aggregates is rotational motion and energy exchange between translational and rotational degrees of freedom during collisions. Rotation of aggregates reduces the chances of penetration of smaller particles into their inner areas which results in lower dimensionality, chain-type structure and local anisotropy. The algorithm described later takes into account these important characteristics of the aggregation process.

At the initial moment in time, all particles are randomly positioned in a rectangular box with the side of about 10^3 times the particle radius and assigned initial velocities according to the the Maxwell distribution. Then mutual potential forces between the particles are introduced and discrete-time simulation of the Newtonian dynamics is performed.

In the absence of a collision, the coordinates and velocity of a particle changes during an iteration step according to $\boldsymbol{r}_i' = \boldsymbol{r}_i + \boldsymbol{v}_i dt$, $\boldsymbol{v}_i' = \boldsymbol{v}_i + (\mathbf{F}_i/m_i)dt$ where $\boldsymbol{r}_i$, $\boldsymbol{v}_i$, m_i, and $\boldsymbol{F}_i$ are the coordinate, velocity, mass, and force that acts on the ith particle, respectively. The force is calculated at each time point t from the total interaction potential. In particular, the algorithm allows one to include the Coulomb and van der Waals interparticle potentials and external potentials such as gravity and external electric fields. In addition, a nonconservative force (viscous friction) is also incorporated into the model. During a collision, all inter-particle interactions are dominated by the short-range van der Waals potentials (which are much stronger than the electrostatic forces). However, after two particles collide, they are assumed to be rigidly connected, and the subaggregates continue to move as rigid bodies for the rest of the aggregation process.

The distances between all pairs of particles are calculated during each iteration step. When the interparticle distance r_{ij} between two particles i and j becomes equal or less than the sphere diameter, these two particles are considered to be rigidly attached to each other. Subaggregates formed in this manner continue to move under the influence of forces acting on each individual particle as rigid bodies. Note that the particle sticking condition is checked *after* an elementary move. This means that they can technically overlap (the distance between particle centers may become smaller than the sphere diameter). However, the time steps are chosen to be sufficiently small (and velocity dependent), so that the depths of such overlaps are small compared to sphere diameters, and when overlaps happen, the interparticle distance is slightly enlarged to the point of exact touching.

An elementary rotation of a subaggregate (with more than one particle) is taken into account with the use of rotation matrices

$$R_x(\alpha) = \begin{pmatrix} 1 & 0 & 0 \\ 0 & \cos\alpha & -\sin\alpha \\ 0 & \sin\alpha & \cos\alpha \end{pmatrix},$$

$$R_y(\beta) = \begin{pmatrix} \cos\beta & 0 & \sin\beta \\ 0 & 1 & 0 \\ -\sin\beta & 0 & \cos\beta \end{pmatrix},$$

$$R_z(\gamma) = \begin{pmatrix} \cos\gamma & -\sin\gamma & 0 \\ \sin\gamma & \cos\gamma & 0 \\ 0 & 0 & 1 \end{pmatrix}.$$

These transformations are applied step by step to all particles in a given subaggregate. The new coordinates as a result of a

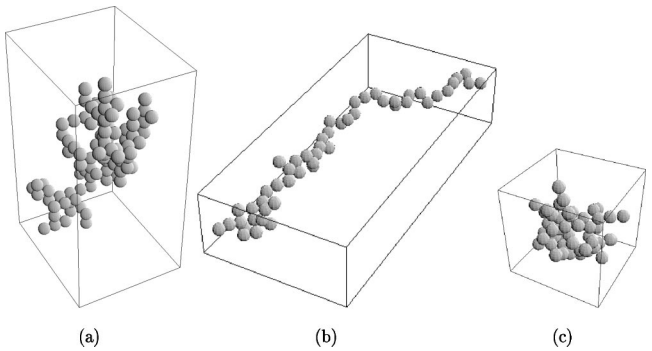

FIG. 1. Sample aggregates used for optical properties calculations: lattice CCA, $D \approx 1.8$ (a); off-lattice, $D \approx 1.3$ (b); and off-lattice, $D \approx 2.3$ (c).

rotation are calculated according to $\boldsymbol{r}_i' = R_x(\alpha)R_y(\beta)R_z(\gamma)\boldsymbol{r}_i$ where $\alpha = w_x dt$, $\beta = w_y dt$, $\gamma = w_z dt$, and $\boldsymbol{w}$ is the angular velocity of an aggregate which satisfies $\hat{I}\boldsymbol{w} = \boldsymbol{J}$ where $\boldsymbol{J}$ is the angular moment and $\hat{I}$ the tensor of inertia of the aggregate being rotated. The angular velocity is calculated from the moment of inertia by inverting the tensor I, namely, $\boldsymbol{w} = \hat{I}^{-1}\boldsymbol{J}$. The linear velocities of individual particles in an aggregate change as the result of rotation according to $\boldsymbol{v}_i' = \boldsymbol{v}_i + \boldsymbol{w} \times (\boldsymbol{r}_i - \boldsymbol{r}_c)$ where $\boldsymbol{r}_c$ is the center of mass of the aggregate. In turn, the angular momentum is updated according to $\boldsymbol{J}' = \boldsymbol{J} + \boldsymbol{M}dt$ where $\boldsymbol{M}$ is the total torque acting on the aggregate being rotated. At the initial time $\boldsymbol{M} = 0$. For an each consequent iteration step, $\boldsymbol{M}$ is found from the known forces that act on each individual particle in a subaggregate: $\boldsymbol{M} = \boldsymbol{M} + d\boldsymbol{M}$; $dM = \Sigma_i \boldsymbol{F}_i \times (\boldsymbol{r}_i - \boldsymbol{r}_c)$.

The described algorithm is capable of simulating the aggregation process for particles of arbitrary size distribution. It allows one to generate aggregates with controlled value of fractal dimension in the range $1 < D < 3$ by means of tuning the parameters of the model. To define the fractal dimension of aggregates D the following expression was used:

$$N = k_0 (R_g/a)^D, \tag{47}$$

where k_0 is a prefactor.

In Fig. 1 we show typical aggregates of each type. The lower-dimensional aggregates ($D \approx 1.3$) were generated under the conditions of relatively stronger anisotropy of the interparticle interactions, while the denser aggregates ($D \approx 2.3$) the centrosymmetrical part of the interaction was enhanced. Note that the aggregate sizes used in simulations of optical properties were insufficient to accurately determine the fractal dimension. The latter was calculated using much larger aggregates of the same type. However, the morphology differences between aggregates with different fractal dimension shown in Fig. 1 are quite apparent. Complete details of the aggregation algorithms will be published elsewhere.

B. Representation of the resolvent as a continued fraction

We have calculated the DOS by using Eq. (16). The resolvent was expressed as a continued fraction[56]

$$\langle E_0 | R(z;W) | E_0 \rangle = \cfrac{\langle E_0 | E_0 \rangle}{z - \alpha_0 - \cfrac{\beta_1^2}{z - \alpha_2 - \ldots}}. \tag{48}$$

The set of coefficients α_n and β_n is obtained from tridiagonalization of the matrix $\langle ilm|W|i'l'm' \rangle$. Namely, starting with $|u_0\rangle = [\langle E_0 | E_0 \rangle]^{-1/2} |E_0\rangle$, we build the orthonormal basis $|u_n\rangle$ in which W is tridiagonal according to the basic Lanczos recursion

$$W|u_n\rangle = \alpha_n |u_n\rangle + \beta_{n+1}|u_{n+1}\rangle + \beta_n |u_{n-1}\rangle. \tag{49}$$

A few notes on the numerical implementation of the earlier method must be made. First, the computationally intensive part of each iteration is a matrix-vector multiplication. The matrix itself is not updated during the iterations. This allowed us to store it in a memory-efficient way using the block structure of Eq. (44). Indeed, the storage of the full matrix may require an exceedingly large amount of memory. For instance, the calculations with $N = 100$ and $L = 64$ will require approximately 714 Gb of memory in double precision if only the upper triangle of W is stored. However, the block structure of W which is apparent from Eq. (44) allows one to store in the memory a few different blocks, each much smaller than W itself, and construct the matrix elements when they are needed by several multiplications. Although this comes at a price of reduced speed, this storage scheme allows one to run this computation in principle, even on a computer with about 0.5 Gb of memory. In the case of lattice aggregates, the memory requirements are even further reduced since many translational vectors $\boldsymbol{r}_{ii'}$ in such aggregates are the same. Second, the matrix W is, strictly speaking, not sparse. However, some of its matrix elements are very small. We have verified that setting $\langle ilm|W|i'l'm' \rangle = 0$ for $r_{ii'} > 4a$ and $l + l' > 2$ does not change the results in any noticeably way. This approximation amounts to neglecting all interaction with multipole orders larger than $L = 1$ between particles whose centers are further apart than two sphere diameters. (Note that the dipole interaction corresponds to $L = 1$ and was taken into account for all pairs of spheres.) Empirically, this increased the computation speed by the factor of three to four times. We have used this approach for large-scale computations of extinction spectra for fractal aggregates in Sec. IV B; the spectra of linear chains (Sec. IV A) were calculated without this approximation. In Fig. 2 we show the relative effect of this approximation on a DOS of a fractal cluster with $N = 50$, $D \approx 2.3$, and $L = 64$. Finally, convergence of the continued fraction (48) itself was confirmed for relatively small systems by direct diagonalization. For large system sizes, the convergence was verified visually. An example of convergence with the order k of approximant to the continued fraction (48) is shown in Fig. 3. It can be seen that the convergence is obtained for $k \approx L = 64$.

IV. RESULTS

A. DOS for linear chains of particles

We start with the simplest case of a chain consisting of only two spheres. The electromagnetic properties of two in-

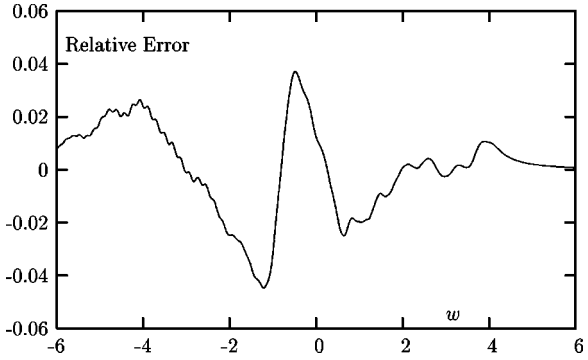

FIG. 2. Relative error $[\Gamma^{(\text{exact})}(w)-\Gamma^{(\text{approximate})}(w)]/\Gamma^{(\text{exact})}(w)$, where $\Gamma^{(\text{approximate})}$ was calculated with the approximation discussed in Sec. III B (setting certain small matrix elements to zero) and $\Gamma^{(\text{exact})}$—without this approximation. Parameters used: $N=50$, $L=64$, $\delta=0.2$.

teracting spherical particles have been studied quite extensively. However, most studies have focused on numerical calculation of optical cross sections or distribution of local fields for a material with given dielectric function (e.g., see Refs. 48 and 70) rather than on calculation of DOS. A few analytical results have been also obtained. Mazets[71] has calculated the electrostatic polarizability of two conducting spheres (the same result may be obtained by the method of images[72]). Paley *et al.*[73] have calculated analytically the quasistatic polarizability of two interacting spheres with arbitrary dielectric permeability. From the results obtained in Ref. 73 an expression for DOS can be deduced, but it appears to be incorrect. In particular, in the case when the external field is parallel to the axis connecting the sphere's centers, it follows from Eq. 32 in Ref. 73 that $\Gamma(w)$ is given by[74]

$$\Gamma(w)=\int_0^\infty f_1(x)\,\delta[w-f_2(x)]dx, \tag{50}$$

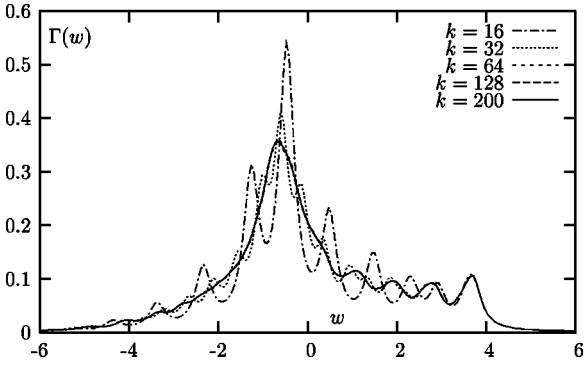

FIG. 3. Illustration of the convergence of the iterative method. The rotationally averaged DOS $\Gamma(w)$ calculated using the continued fraction representation (48) is plotted as a function of w for the continued fraction terminated at different levels k. Calculation was performed for a single off-lattice aggregate with $N=50$ and $D\approx 1.3$. Other parameters: $L=64$ and $\delta=0.2$. Note that the curves $k=64$, $L=128$, and $k=200$ are practically indistinguishable.

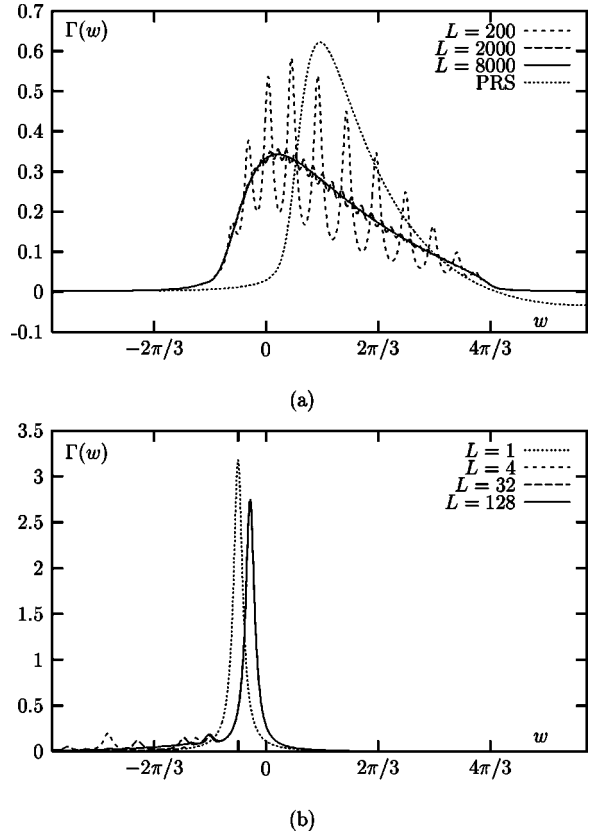

FIG. 4. DOS for two touching spheres for different values of L and polarization of external field parallel (a) and perpendicular (b) to the line connecting the sphere centers. The relaxation parameter is set to $\delta=0.1$. PRS—result of Paley *et al.*[73]

$$f_1(x)=x(x-1)\exp(-x),\quad f_2(x)=\frac{4\pi}{3}\frac{1+(x-1)\exp(-x)}{x}, \tag{51}$$

which can be equivalently rewritten as

$$\Gamma(w)=\begin{cases}-f_1[g(w)]g'(w), & \text{if } 0\leqslant w\leqslant 8\pi/3\\ 0, & \text{otherwise}\end{cases}, \tag{52}$$

where $g(w)$ is the solution to the nonlinear equation $f_2(g)=w$ and prime stands for differentiation. It can be seen that this expression results in nonzero (and, actually, negative) values for $\Gamma(w)$ for $w>4\pi/3$, which contradicts both the property of the DOS derived in Sec. II C 1 and the Hermiticity of the operator W and can, for example, result in negative values of the extinction cross section for dielectric scatterers in the long wavelength region.

We have calculated the DOS for two touching spheres numerically. The result is shown in Fig. 4. In this figure we illustrate the convergence of results with L, and also plot for comparison the DOS given by Paley *et al.* [calculated by numerical integration according to Eq. (50) where the delta function was replaced by a Lorentzian with the same value of δ as in the other plots].

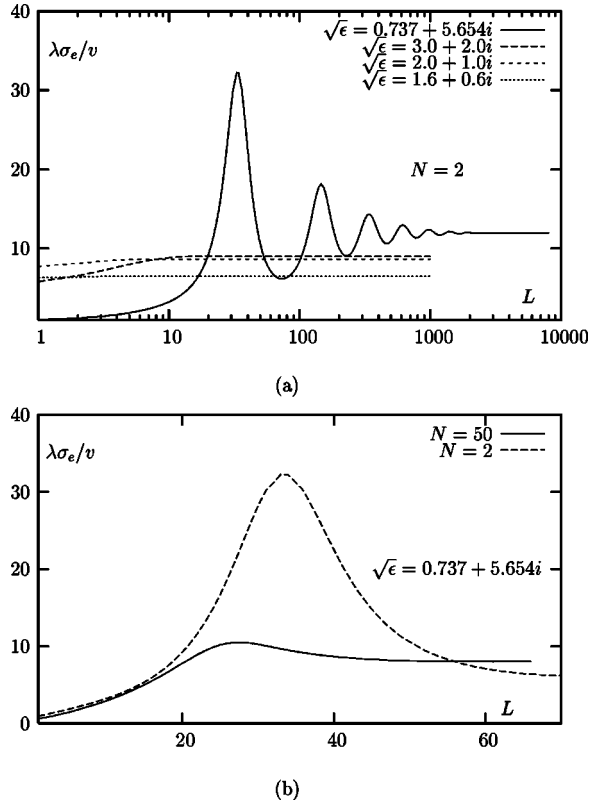

FIG. 5. Convergence of the dimensionless quantity $\lambda\sigma_e/v$ with L for different values of the complex refractive index $\sqrt{\epsilon}$. (a) Two touching spheres with polarization of the incident field parallel to the axis for different values of $\sqrt{\epsilon}$. (b) Two touching spheres compared to a random off-lattice aggregate with $N=50$ for $\sqrt{\epsilon}=0.737+5.654i$.

When the external field is polarized parallel to the axis connecting the particle centers [Fig. 4(a)], the convergence with L appears to be slow. This is explained by the fact that the system is highly degenerate due to the cylindrical symmetry so that only modes with $m\neq 0$ give input to the DOS. Due to the same reason, we have been able to calculate $\Gamma(w)$ for extremely large values of L. The convergence with L is illustrated in a more quantitative way in Fig. 5. Here we plot the dimensionless quantity $\lambda\sigma_e/v$ for two touching spheres as a function of L for different values of the refractive index $\sqrt{\epsilon}$ (the same values are used in Table I later) and the polarization parallel to the axis. It is evident, both from Figs. 4 and 5, that the DOS eventually converges to a well-defined limit. It also satisfies the requirement formulated in Sec. II C 1. Note that a much faster convergence is expected in the absence of axial symmetry when and all modes with $m\neq 0$ make an input to the DOS. This is indeed confirmed by simulations, as shown in the Fig. 5(b), where two spheres are compared with a random off-lattice aggregate with $N=50$ and $D\approx 2.5$ for the value of $\sqrt{\epsilon}$ used in Fig. 5(a) which resulted in the slowest convergence. We see that for this value of $\sqrt{\epsilon}$ convergence is reached for $L\sim 4000$ in the case of two spheres but already for $L\sim 60$ in the case of a random aggregate.

Now we return to the discussion of Fig. 4(a). The full multipolar DOS for two touching spheres is dramatically different from the DOS in the DA. Thus, in the case $L=1$ (dipole terms only), DOS contains a single peak of width δ centered at $w=\pi/3$. The true DOS is much wider spanning the interval from approximately $-\pi/3$ to $4\pi/3$. It is interesting to note that it extends to the theoretical right bound $4\pi/3$, and, judging from the plot, a scaling dependence of the form $\Gamma(w)\approx(4\pi/3-w)^{\alpha}$ for $w<4\pi/3$ is plausible. The results obtained with the account of high-order multipolar interactions indicate a strong absorption by a two-sphere aggregate at the resonance frequency of an isolated sphere (the Frohlich frequency). This effect was not described theoretically before and is of special interest. In particular, calculations within the GCRM consistently resulted in smaller absorption at the Frohlich frequency than was experimentally measured.[2,10,57,58] However, the account of high-order multipolar interactions corrects this discrepancy. Physically, this can be understood by observing that, contrary to the assumptions of the DA, the internal fields in a two-sphere aggregate contain components both parallel and perpendicular to the axis connecting the sphere centers, even if the external field is parallel to this axis. We will also see later that the relatively high absorption at the Frohlich frequency, compared to that predicted by the GCRM, is also characteristic for multisphere random aggregates.

For polarization of the external field orthogonal to the axis [Fig. 4(b)], interaction is much weaker. This fact is

TABLE I. The ratio $\sigma_e/\sigma_e^{(\mathrm{nonint})}$, where $\sigma_e^{(\mathrm{nonint})}=4\pi kNa^3\mathrm{Im}[(\epsilon-1)/(\epsilon+2)]$, for different values of the refractive index $\sqrt{\epsilon}$ and the number of spheres in the chain, N. The maximum order of spherical harmonics is as follows. (a) $L_{\parallel}=8000$ for $N=2$ and $L_{\parallel}=4000$ for all other N and $L_{\perp}=128$ (here $L_{\parallel}$ is used for polarization parallel to the chain axis and $L_{\perp}$—for orthogonal polarization); (b) $L_{\parallel}=L_{\perp}=10$. Column (M): data adopted from Fig. 6 in Ref. 48.

	$\sqrt{\epsilon}=1.6+0.6i$			$\sqrt{\epsilon}=2+1i$			$\sqrt{\epsilon}=3+2i$			$\sqrt{\epsilon}=0.737+5.654i$	
N	(a)	(b)	(M)	(a)	(b)	(M)	(a)	(b)	(M)	(a)	(b)
2	1.033	1.034	1.03	1.106	1.106	1.11	1.410	1.393	1.38	8.445	2.679
3	1.054	1.054	1.05	1.176	1.177	1.19	1.748	1.724	1.71	17.36	5.195
4	1.067	1.067	1.05	1.220	1.221	1.22	1.991	1.966	1.91	25.41	8.228
5	1.075	1.075	1.06	1.250	1.251	1.26	2.166	2.141	2.09	31.82	11.47
10	1.093	1.058	1.07	1.315	1.319	1.32	2.570	2.967	2.49	46.78	57.27
∞	1.035	1.058	1.10	1.290	1.319	1.38	2.945	2.967	2.90	62.76	57.27

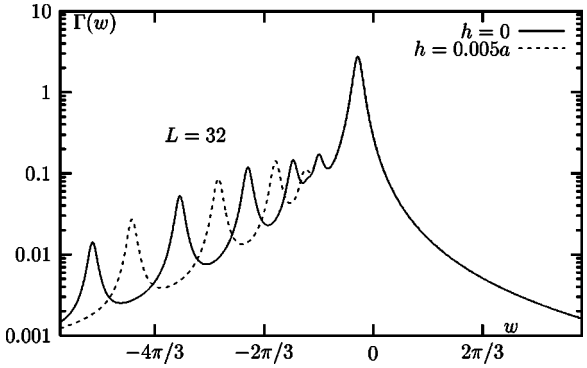

FIG. 6. Dependence of the DOS for two spheres on the separation h between the spheres. The polarization of external field is orthogonal to the line connecting the sphere centers; $L=32$, $\delta=0.1$.

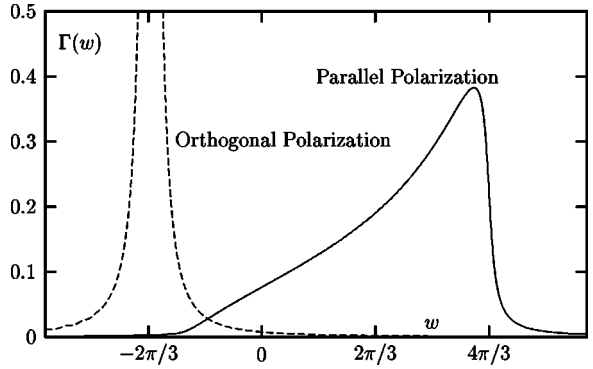

FIG. 7. DOS for an infinite chain of spheres for polarization parallel (solid line) and orthogonal (dashed line) to the chain. The top part of the peak corresponding to the orthogonal polarization is not shown (the peak height is approximately 3.1). The relaxation parameter is set to $\delta=0.1$; $L=8000$ for parallel polarization and $L=128$ for orthogonal polarization.

widely known (see, for example, Ref. 71). However, the analysis of DOS provides an additional insight into the nature of interaction. It can be seen that, similar to the DA, there is a well-pronounced single peak. However, it is shifted from the value predicted by the DA ($w=-\pi/6$) toward the resonance of an isolated sphere; the maximum is approximately at $w=-\pi/10$. The convergence of DOS with L at this central peak is very fast and is reached already for $L=4$. However, there are also additional peaks in the negative w region. The amplitudes of these peaks are much smaller than that of the main peak, and they are not fully converged. In fact, these peaks are extremely sensitive to the details of local geometry, as is illustrated in Fig. 6. In this figure we plot DOS for two touching spheres and for two spheres separated by a distance $h=0.005a$ (between the two nearest points). While the main peak is practically insensitive to this separation, the smaller peaks completely change their positions. It can be argued that in any real physical system such peaks must be smoothed out due to imperfections of the surface, effects of nonlocality of the dielectric permeability, dispersion of particle sizes, etc.

Next we consider linear chains of particles. Infinite chains can be introduced into calculations by replacing the terms $(a/r_{ii'})^{l+l'+1}$ in Eq. (44) by the Riemann ζ functions $\zeta(s)=\Sigma_{i=1}^{\infty} i^{-s}$ where $s=l+l'+1$. The DOS of an infinite chain is shown in Fig. 7. Obviously, it is very different both from the DOS in the dipole approximation and the DOS for two spheres. First, consider the case of external polarization parallel to the chain. In this case DOS has a maximum at $w=4\pi/3$ and is discontinuous at this point, so that $\Gamma(w)=0$ for $w>4\pi/3$. The discontinuity of DOS at $w=4\pi/3$ is expected, since the electrostatic polarizability of an infinite chain is infinite and, as discussed in Sec. II C 2, the DOS can be nonzero in this case at $w=4\pi/3$; however, it must be identically zero for $w>4\pi/3$. Note that the depolarization coefficient corresponding to $w=4\pi/3$ is $\nu=1/3-w/4\pi=0$, which is the same as in an infinite cylinder for polarization parallel to its axis. However, the DOS for an infinite cylinder has only one peak (for parallel polarization) centered at $w=4\pi/3$ while the DOS for an infinite chain of spheres is strongly broadened and forms a continuous band in the region $-2\pi/3<w<4\pi/3$. This constitutes the major difference between electromagnetic properties of linear chains of spheres and and prolate spheroids which was established earlier in Ref. 48. Now we turn to polarization orthogonal to the chain. In this case DOS has a single peak centered near $w=-2\pi/3$. This value of w corresponds to $\nu=1/2$ which is the depolarization coefficient of an infinite cylinder for polarization orthogonal to its axis. Note that the exact position of the peak shown in Fig. 7 is shifted from $w=-2\pi/3$ toward $w=0$ by about 2%, but is not broadened, at least its widths in not larger than $\delta=0.1$ which was the value of the relaxation constant used in the calculations. Thus, the linear electromagnetic properties of an infinite chain of spheres are very close to those of an infinite cylinder when polarization is orthogonal to the axis. For polarization parallel to the axis, linear spectra of these two objects may have the same main features (the position of the maximum, decrease or increase of absorption with the wavelength), but are quantitatively different.

The DOS of finite chains is intermediate between the $N=2$ and $N=\infty$ cases and depends on N as illustrated in Fig. 8. The DOS maximum gradually shifts as N grows from $w=0$ to $w=4\pi/3$ for the parallel polarization of the external field and from $w\approx-\pi/10$ to $-2\pi/3$ for the orthogonal polarization. This is explained by the fact that the higher multipolar interactions are short range. When the length of the chain increases, the relative influence of the long-range dipole interaction also grows. However, the higher multipolar interactions retain significance even in the limit $N\to\infty$, as can be seen from a the differences between the exact and the DA DOS. Note that the rotationally averaged DOS for an infinite chain and two touching spheres is shown in Sec. IV B later (Fig. 11).

We have also calculated the extinction cross section for several values of the refractive index of the material and different lengths of the chain. Such calculations were carried out earlier [48] and provide us with a means to validate the numerical procedures used in this paper. The results are displayed in Table I. The quantity shown is the dimensionless ratio $\sigma_e/\sigma_e^{(\mathrm{nonint})}$ where $\sigma_e^{(\mathrm{nonint})}=4\pi k\, Na^3\mathrm{Im}[(\epsilon-1)/(\epsilon+2)]$ is the extinction cross section for N noninteracting spheres, and all cross sections are rotationally averaged (the same

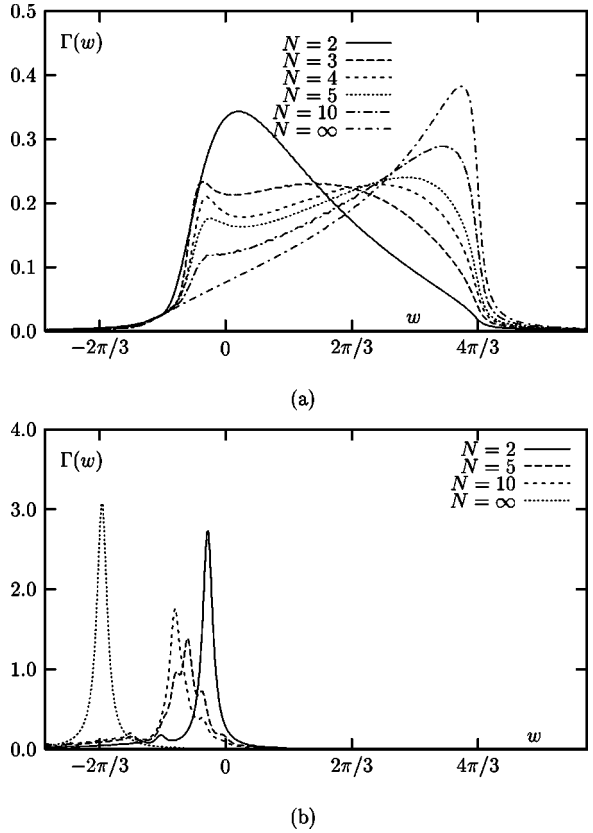

FIG. 8. DOS for chains of different length for polarization parallel (a) and orthogonal (b) to the axis; $\delta=0.1$.

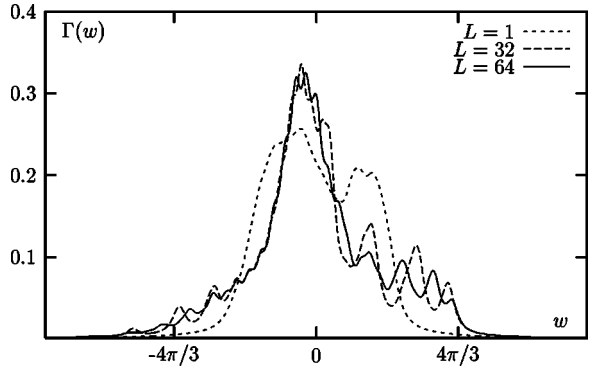

FIG. 9. DOS for lattice CCA aggregates for different values of L. The relaxation constant is set to $\delta=0.2$. Averaging performed over five random realizations of aggregates and over rotations.

quantity as in Fig. 6 of Ref. 48). Fully converged results for very large values of L (as specified in the caption) are given in columns labeled (a). Results for $L=10$, which in some cases are not fully converged, are in columns labeled (b). The columns labeled (M) contain data obtained by digitization of Fig. 6 in Ref. 48. Our results coincide with those of Ref. 48 within the precision allowed by digitization of Fig. 6 in Ref. 48 (approximately, 3%). However, some discrepancies remain. We note that there is a slightly better match between the data in columns (b) and (M) than between data in columns (a) and (M). Discrepancies are the strongest in the $N=\infty$ case which is not calculated directly in Ref. 48 (instead, we used the data for $N=100$).

The first three values of $\sqrt{\epsilon}$ shown in the table correspond to $\mathrm{Re}(\epsilon)>0$. As is discussed in Sec. II C 2, the parameter X in this case is greater than $4\pi/3$, so that the DOS at $w=X$ is identically zero. As a result, electromagnetic excitation of such materials is off-resonance. In particular, interaction is weak and convergence with L is fast. Indeed, we have found that $L=10$ already provides a result accurate within 3% for these three values of $\sqrt{\epsilon}$. Also, the numerical value of the ratio $\sigma_e/\sigma_e^{(\mathrm{nonint})}$ is close to unity, which is a manifestation of the relatively weak interaction. The situation changes dramatically when $\mathrm{Re}(\epsilon)<0$ and, correspondingly, $X<4\pi/3$. In this case the DOS can be nonzero at $w=X$ and resonance excitation can take place. To illustrate this, we chose the fourth value of $\sqrt{\epsilon}$ to be $\sqrt{\epsilon}=0.737+5.654i$ which corresponds to silver at $\lambda=818$ nm with the finite-size corrections for $a=5$ nm as discussed later in Sec. IV D. Note that for this value of the refractive index $X\approx 0.9(4\pi/3)$ and $\delta\approx 0.09$. At $N=\infty$, the ratio $\sigma_e/\sigma_e^{(\mathrm{nonint})}$ is 62.76—more than 30 times larger than in any of the three preceding cases. As can be expected, a much larger value of L is required for convergence in this case.

An interesting topic discussed in Ref. 48 was a comparison of the extinction cross section of an N-sphere chain and a prolate spheroid with the same aspect ratio. It was shown that prolate spheroids are more efficient absorbers for the first three values of $\sqrt{\epsilon}$ shown in Table I. We can conclude by examining Fig. 8 that this is generally true when $X>4\pi/3$ because the DOS for longitudinal modes of a chain is always shifted in the "integral sense" toward $w=0$ compared to the DOS of prolate spheroid with the same aspect ratio, while transverse modes can be neglected for $X>0$. However, the effect is expected to be opposite for materials with $\mathrm{Re}(\epsilon)<0$ and $X<4\pi/3$. Consider, for example, $\sqrt{\epsilon}=0.737+5.654i$. In the limit of $N\to\infty$, when the disparity between chains and prolate spheroids was shown to be strongest,[48] we have for this refractive index (after rotational averaging) $\sigma_e/\sigma_e^{(\mathrm{inf.cyl.})}\approx 1.8$.

B. DOS for fractal aggregates

We start with the DOS of lattice cluster-cluster aggregates. We have performed computations for aggregates with $N=100$ particles and for values of L up to $L=64$. Note that the size of the associated linear system is approximately 422 000 equations with complex coefficients, or 844 000 real equations.

The DOS (averaged over five random aggregate realizations and over rotations) is illustrated in Fig. 9 for different values of L. It can be seen that the central peak near $w=0$ has converged quite satisfactorily at $L=64$. However, there are some nonconverged oscillations in the tails of the DOS. The oscillations in the region $3<w<4$ are physically important since the value of $\Gamma(w)$ in this interval determines the IR and far IR absorption of metal colloid aggregates. The oscillations are similar to the ones observed in bispheres in orthogonal polarization and the amplitude of these oscillation decreases with L. It is obvious, however, that the nonzero

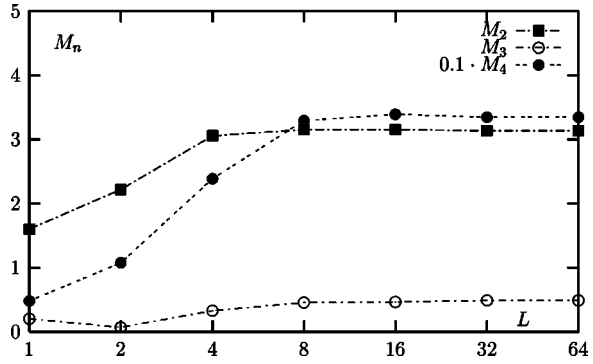

FIG. 10. First few moments M_n of the DOS for CCA aggregates as functions of L. ($M_0=1$ and $M_1=0$ identically for any L.)

DOS extends almost to the critical value of $w=4\pi/3$. This is a very important fact indicating that the collective resonant extinction of metal colloid aggregates will extend very far into the IR.

Despite some nonconverged features, the qualitative shape of the DOS is quite evident from Fig. 9. The true DOS differs from the DA DOS quite substantially. In particular, the true DOS retains a higher value near the resonance of an isolated particle than the DA predicts. This may account for the experimental observation of a spectral peak near the Frohlich wavelength in fully aggregated metal colloid aggregates which could not be adequately understood within the DA.[57,58] However, for the values of w close to the right bound of $4\pi/3$, the DOS obtained in the DA is zero, while the true DOS remains finite. The second moment M_2 (characteristic width) of the true DOS is larger than that of the DA DOS. Convergence with L of the first few moments of DOS, $M_n \equiv \int w^n \Gamma(w) dw$, is illustrated in Fig. 10. Note that $M_0=1$ and $M_1=0$ identically for all values of L. The moments shown in Fig. 10 are obviously converged. However, convergence of higher moments is slower. In general, we have verified that the higher is the order of the moment, the larger value of L is required for its convergence. Thus, taking higher values of L leads to changing the shape of the DOS on finer and finer scales. For any given value of δ, convergence with L is reached when this scale becomes much smaller than δ. (When the continued fraction representation (57) is used to calculate DOS, the order of the approximant, k, must be larger than $[n/2]+1$, regardless of L, in order to obtain an accurate value for $M_n(L)$.)

The DOS for five random CCA aggregates is compared to that of an infinite chain and a bisphere (averaged over rotations) in semilogarithmic scale in Fig. 11. The DOS for the CCA aggregates and bispheres share some similarity. However, it is obvious that everywhere except for a narrow central peak (slightly shifted from $w=0$ to the left), aggregates are more effective absorbers than bispheres. This result is explained by the relatively high input of bispheres with the axis perpendicular to polarization of the external field to the rotationally averaged spectra. However, in the region $0<w<2$ the two curves are very similar, which prompts that binary interactions are dominating in this interval of w's. The infinite chains have DOS which is distinctly different from that of aggregates and bispheres: it is significantly smaller at $w=0$ but larger at $w=4\pi/3$.

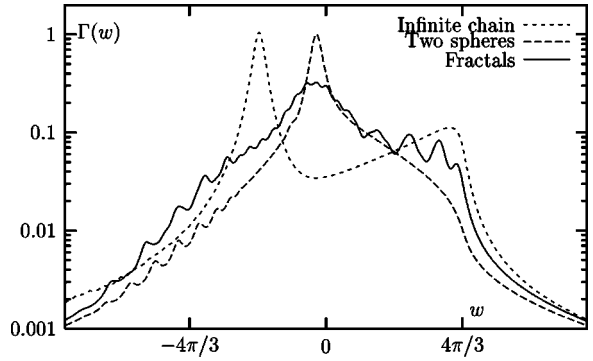

FIG. 11. Comparison of the DOS for a lattice CCA aggregates (averaged over five random realizations), a bisphere, and an infinite chain of spheres. All curves are rotationally averaged; $\delta=0.2$.

Next we consider the dependence of the DOS on the fractal dimension and type of aggregates. DOS for different types of aggregates is shown in Fig. 12. One can see that all curves are qualitatively similar. The main peak of the curve $D\approx 1.3$ (low-dimensional aggregates) is visibly shifted to the left from the other two peaks. Also, the difference is well manifested near $w=4\pi/3$, which has important implications for long wavelength behavior of extinction. More specifically, the DOS for aggregates with $D=1.8$ near the critical point $w=4\pi/3$ is higher than for the other two types of aggregates. This means that the CCA aggregates are more efficient absorbers in the IR and far IR. It is not clear if this is the consequence of the particular value of the fractal dimension, or of the local structure of the aggregates. Also, it is obvious that in the case of the more dense aggregates ($D\approx 2.3$), the DOS is more smooth and appears to be better converged.

C. Comparison with the geometrical cluster renormalization method

The GCRM was proposed in Refs. 57 and 58 and used consequently in a number of papers (for example, see Refs. 2, 3, 6, 10, 22, 39, and 59–62). It is described in detail in Refs. 51 and 52. The method allows one to capture some important features of the collective electromagnetic interac-

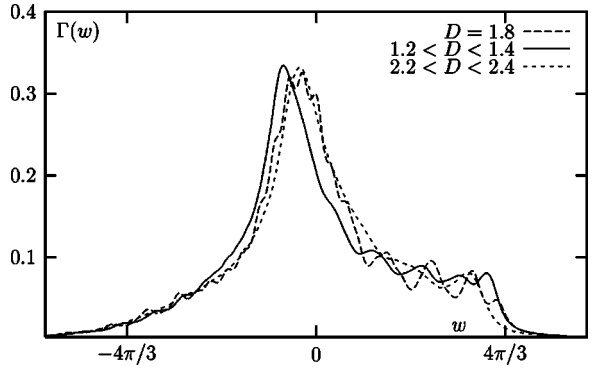

FIG. 12. Comparison of the DOS for lattice CCA ($N=100$, $D\approx 1.8$) and for off-lattice aggregates with $N=50$ and $D\approx 1.3$ and $D\approx 2.3$. $L=64$; $\delta=0.2$.

tion in an aggregate while staying within the DA. It has been validated qualitatively by comparison with experimental data (e.g., see Refs. 2, 3, 10, and 39), but not with rigorous simulations. In particular, the main features of experimentally observed absorption spectra of silver colloid aggregates were described within the GCRM quite adequately.[2,8,10,11] The method is briefly summarized later. The central idea of GCRM is to replace (for the purpose of numerical simulations) an ensemble of aggregates with experimental parameters by an ensemble with different average number of particles in an aggregate (N), different radius of a single particle (a) and different distance between centers of the nearest neighbor particles (l). Geometrical intersections of nearest neighbor spheres is introduced and an intersection parameter ξ is defined as the ratio of the distance between centers of two nearest neighbor spheres to the sphere radius. In an aggregate of touching spheres $\xi=2$ while in a renormalized aggregate $\xi<2$. The set of transformations $a'=a(\xi/2)^{D/(3-D)}, N'=N(2\xi)^{3D/(3-D)}, l'=\xi a'$, defined for an arbitrary $\xi\in(0,2]$ and fractal dimension $D\in[0,3)$, keeps the total volume of the scattering material, the average gyration radius of aggregates in an ensemble, and the fractal dimension unchanged. These three parameters are considered to be important statistical characteristics of an ensemble of aggregates. The choice of parameter ξ is somewhat phenomenological. The following two choices have been used in the literature. First, $\xi=(4\pi/3)^{1/3}\approx 1.612$ follows from an analogy with the discrete-dipole approximation.[75] If we place centers of the spheres on a cubic lattice, This value of ξ provides that the volume of a single sphere is equal to that of a single cubic cell, so that the volume fill fraction is 1. The second value, $\xi\approx 1.688$ was obtained from the requirement that a linear chain of spheres has the same depolarization factors as an infinite cylinder.[76] In addition, $\xi\approx 1.788$ can be obtained from the requirement that the renormalized DOS has the same second moment M_2 as the multipole DOS (the latter is shown in Fig. 10).

In the quasistatic limit, the earlier set of transformations is mathematically equivalent to replacing the original DOS obtained in the DA, $\Gamma_{\mathrm{DA}}(w)$, by $\Gamma'(w)=(2/\xi)^3\Gamma_{\mathrm{DA}}[(\xi/2)^3 w]$ (note that no such simple scaling rule for the DOS exists beyond the quasistatics). In Fig. 13 we compare the multipole DOS ($L=64$) calculated for an ensemble of five lattice CCA aggregates containing $N=100$ particles each with that obtained with the GCRM for different intersection parameters ξ. It can be concluded from the data plotted in Fig. 13 that the renormalized DOS does not resemble the multipole one for all values of w. Most importantly, the renormalized DOS does not posses a central peak near $w=0$. Perhaps this fact explains that the approaches based on the GCRM did not describe properly absorption near the Frohlich frequency in silver colloidal aggregates.[57,58] However, the positive-w wing which describes the long wavelength absorption is described quite adequately by the GCRM. An especially good fit is obtained for $\xi=1.688$.

D. Extinction spectra

Despite some nonconvergent features in the DOS of fractal aggregates, we can conclude from Fig. 5 that $L=64$ is sufficient for obtaining accurate results for the extinction cross section of metals such as silver (with the account of finite-size effects which tend to lower the resonance quality) for the wavelength up to ~800 nm. In this section, we show our results for extinction spectra of aggregates of different materials. In the case of silver we extend the spectral range to approximately 2 μm, a wavelength for which convergence with L has not been established due to computational limitations.

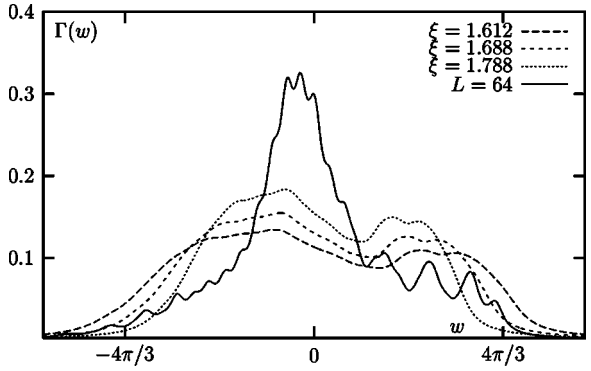

FIG. 13. Comparison of the DOS for CCA aggregates calculated in the GCRM with different intersection parameters and for $L=64$. The second moments of the DOS coincide for the curves $\xi=1.788$ and $L=64$.

First, we show extinction spectra for some lower conductivity metals, namely, iron and palladium. The results of multipole calculations are shown in Fig. 14 and compared with the pure DA and the GCRM. Calculations illustrated in Fig. 14 were carried out for two ensembles of off-lattice aggregates with different fractal dimensions. The function shown is the specific extinction $\epsilon_e=v^{-1}\sigma_e$ (the extinction cross section per unit volume) which has the units of inverse length. Experimental dielectric function of iron and palladium from Refs. 77 and 78 were used. The spectral range in which it was measured in Refs. 77 and 78 determines the spectral range of the specific extinction shown in Fig. 14. The full multipole calculations ($L=64$) are shown by squares, the pure DA by circles and the GCRM approximation with $\xi=1.688$ by triangles. The noninteracting limit (extinction spectra of isolated small spheres) are shown by solid lines for comparison. Note that the noninteracting and pure DA results do not differ significantly for these metals. The difference between the multipole calculations and the DA becomes quite apparent in the long wavelength limit. But GCRM with $\xi=1.688$ provides a very good approximation in the whole spectral range shown in the figure, based on comparison with the $L=64$ curve. The authors are not aware of experimental spectra measured for fractal nanoaggregates built of lower conductivity metals; therefore, no comparison with experimental results is possible at this time. Due to this reason, a GCRM curve with $\xi=1.612$ is not shown in Fig. 14. We only mention that the latter differs significantly from the $L=64$ curve; however, we show later based on comparison with experimentally measured spectra that GCRM with $\xi=1.612$ may provide a better approximation for black carbon and silver in the spectral regions where convergence of the multipole solution with L has not been demonstrated.

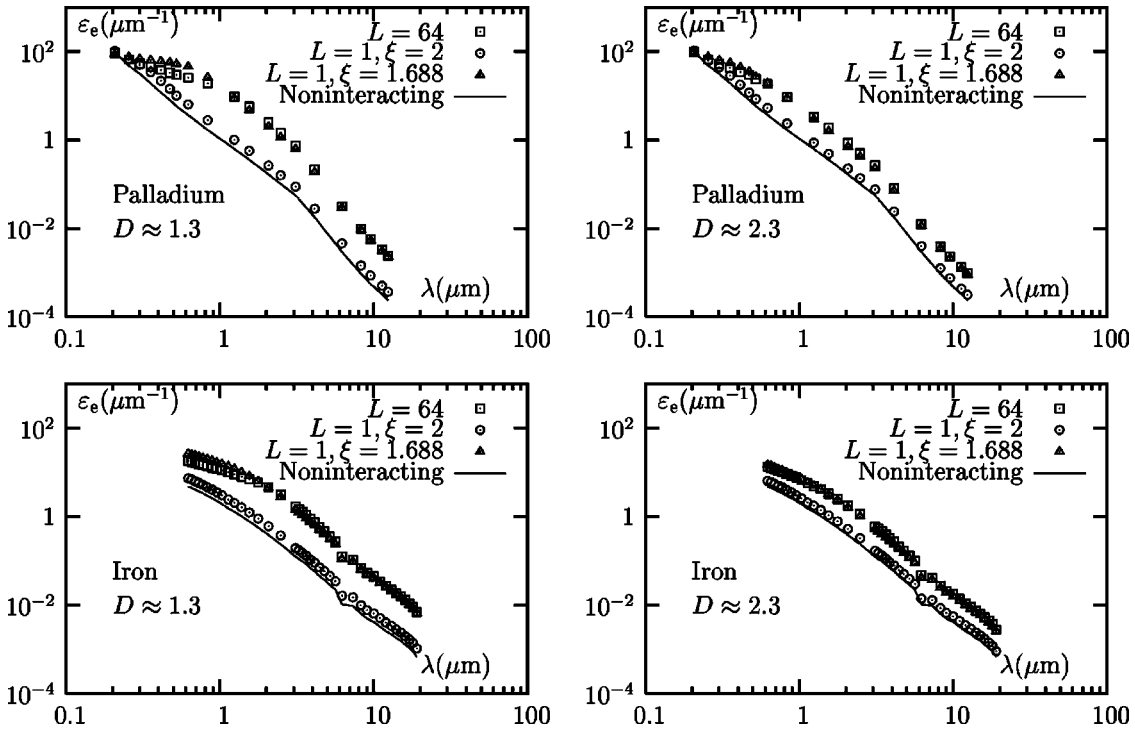

FIG. 14. Extinction spectra of palladium and iron aggregates. Calculated for off-lattice aggregates with different fractal dimensions, as labeled.

Next, we consider aggregates of black carbon. Carbonaceous soots with fractal structure are important atmospheric pollutants and their extinction properties in a wide spectral range are of considerable interest. Absorption spectrum of carbonaceous diesel soot has been measured in a very wide spectral range (from 0.5 μm to 0.857 cm) in Ref. 79. It was demonstrated that neither the model of isolated spheres nor of long cylinders can explain the absorption properties of soot, in particular, the resonance absorption extending into the centimeter spectral region. The latter property was described within the GCRM in Ref. 52. An accurate fit with experimental data was obtained for the intersection parameter $\xi=1.612$. In Fig. 15 we plot the same curves as in Ref. 52 (Fig. 7) and the results for $L=64$ and GCRM with $\xi=1.688$. The plots are shown in the same units and spectral range, and the dielectric function of black carbon is calculated using the same three-electron dispersion formula with parameters given in Ref. 80 as in Ref. 52. However, note that no accurate measurements of the dielectric function of black carbon which constitutes soot, which may limit the accuracy of calculations. Similar to Ref. 52, the experimental data of Ref. 79 were converted from specific extinction per unit mass to specific extinction per unit volume assuming that the mass density of black carbon is 1.9 g/cm^3.

Let us focus on the case $D \approx 1.8$ which is the fractal dimension corresponding to that of aggregates studied in Ref. 79. First, it can be seen that for $\lambda < 100$ μm, the curves $L=64$ and $L=1$, $\xi=1.612$ and $L=1$, $\xi=1.688$ are in reasonable agreement with each other and the experimental data. At the same time, the noninteracting limit (which in this case closely coincides with the pure DA) gives systematically lower absorption starting from approximately $\lambda=2$ μm. However, the curves $L=64$ and $L=1$, $\xi=1.688$ do not provide a good fit to the experimental data in the region $\lambda > 100$ μm. In fact, the difference is quite dramatic at $\lambda \sim 1$ cm. Note that the discrepancy at this wavelength is so large that it cannot be correcting by varying parameters such as the mass density of black carbon in the diesel soot (which was not measured directly). However, the GCRM curve with $L=1$, $\xi=1.612$ provides a reasonably accurate fit to the experimental data (this is also true for $D \approx 2.3$). This is in agreement with the results of Ref. 52.

It is clear from Fig. 15 that the results of multipole calculations ($L=64$) are inaccurate for $\lambda > 100$ μm. This can take place due to one of the following two reasons. First, one can argue that the Ohmic losses (and the value of δ) in black carbon become sufficiently small at these wavelength so that the inaccuracy in the calculated multipole DOS, which can be attributed to insufficiently large value of L, leads to the inaccuracy in calculated spectra. Indeed, it follows from the three-electron formula for the dielectric function of soot that $\delta \sim 10^{-3}$ at $\lambda=1$ cm. However, convergence with L was only obtained for $\delta \sim 0.1$, which corresponds approximately to $\lambda=100$ μm. Note that multipole calculations provide a good agreement with the experimental data for $\lambda < 100$ μm. Then it would follow that the GCRM with $\xi=1.612$ provides, in fact, a better approximation to the true DOS near the critical point $w=4\pi/3$ than the full multipole model. Theoretically, the inaccuracy of the multipole calculations can be corrected by taking even larger values of L and improving numerical methods. However, it seems exceedingly difficult to reach convergence for δ as small as 10^{-3}. The second possible reason is more physical: namely, the three-electron dispersion formula adopted from Ref. 80 may be inaccurate at

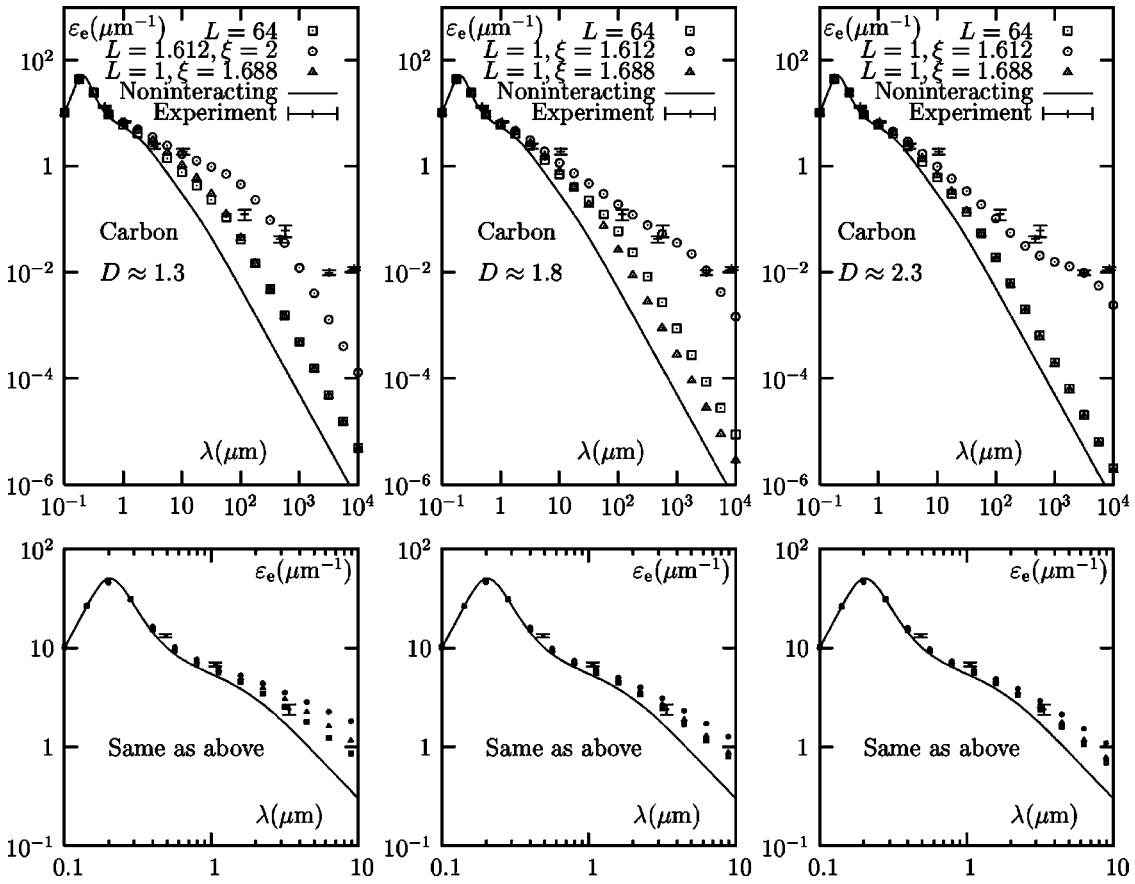

FIG. 15. Extinction spectra of black carbon aggregates. Calculated for lattice and off-lattice aggregates with different fractal dimensions, as labeled. Experimental data adopted from Ref. 79 are shown by error bar symbols. The lower row of plots shows the same spectra as in the plots directly above, but in a smaller spectral range.

large wavelengths. In fact a strong indication of that is the fact that the linear regression of the experimental data of Ref. 79 reveals the power law $\varepsilon \propto 1/\lambda^{\alpha}$ where $\alpha = 0.81 \pm 0.04$. Assuming that this power decay extends to infinitely large values of λ, we would obtain a contradiction with the sum rule (20). Thus, there must be a crossover to a faster decay at some value of λ (which is, perhaps, out of the experimentally attainable range). Such a crossover would indicate that there are additional low-frequency resonances in the dielectric function which are not accounted for in the dispersion formula adopted from Ref. 79. At this point, we can conclude based on the available experimental data that in the spectral range $\lambda > 100$ μm, the GCRM with $\xi = 1.612$ is a better approximation then the multipole calculations, even with the relatively large number of multipoles included ($L = 64$). This finding underscores the importance of the GCRM for highly conducting materials, when the full multipole calculations with the desired degree of precision are not yet feasible.

For the study of certain physical phenomena, such as strong enhancement of optical nonlinearities in fractal aggregates, high conductivity metals such as silver or aluminum are of primary interest. Unfortunately, our multipole calculations lack precision at this time to obtain accurate spectra for these metals for $\lambda > 900$ nm. However, quantitative results can be obtained for shorter wavelengths. We have used the dielectric function for silver given in Ref. 81 with the finite-size correction for the dielectric function. The finite-size correction is obtained by extracting the Drude part from the total dielectric function of silver and replacing the Drude relaxation constant γ_{inf} (which is measured in bulk samples) with $\gamma(a) = \gamma_{\text{inf}} + v_F/a$, where v_F is the Fermi velocity and a the radius of the sphere. The account of the finite-size effects is important for high-conductivity metals (with very small values of γ_{inf}). For silver, $v_F \approx 0.0047c$, (c being the speed of light), $\gamma_{\text{inf}} \approx 0.0019\omega_p$ and the wavelength at the plasma frequency ω_p is $\lambda_p = 2\pi c/\omega_p \approx 136$ nm. We have calculated the finite-size correction for $a = 5$ nm. The account of this corrections effectively increases the value of $\delta(\lambda)$ and leads to a better convergence of the spectra with L. The results, averaged over five random realizations of CCA aggregates with $N = 100$ and over rotations, are shown in Fig. 16. We can conclude that the GCRM curves with both $\xi = 1.612$ and $\xi = 1.688$ are qualitatively compatible with the $L = 64$ results, while the pure DA approximation is obviously inadequate. Most importantly, we see that in the spectral range considered, these three curves demonstrate strong resonance absorption, which is evident from the comparison with the DA and noninteracting curves (in the latter two cases, no resonant excitations are present for $\lambda > 0.5$ μm). The $L = 64$ and the GCRM curves are also in qualitative agreement with the many experimental spectra obtained for silver.[2,8,10,11,57,58] In particular, the second long wavelength spectral peak was ob-

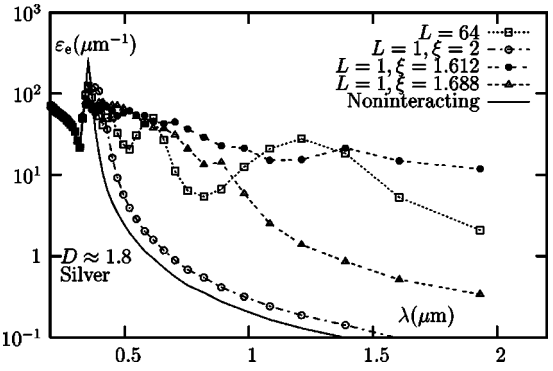

FIG. 16. Extinction spectra of silver aggregates calculated for five lattice CCA aggregates with $N=100$ and $D\approx 1.8$, averaged over rotations.

served in many experiments. A detailed comparison with extensive measurements is beyond the scope of this paper and will be done elsewhere.

V. SUMMARY AND DISCUSSION

In this paper we have solved the quasistatic scattering problem for fractal and regular arrays of touching spheres. The mathematical formalism was based on the electromagnetic DOS. This approach was used earlier within the frame of the DA. Here we have extended this treatment beyond the DA and calculated the DOS and extinction spectra for aggregates built of various materials for the maximum multipole order L up to 64 and for number of particles in an aggregate N up to 100. The values of these parameters used previously in computer simulations were significantly smaller. Note that the number of equations that couples multipole excitations in the array of interacting spheres scales as $NL(L+2)$. We have been able to perform calculations for these relatively high values of N and L due to the computational efficiency of the numerical method in this paper which is based on a continued fraction expansion of the resolvent and an efficient data storage scheme.

The computational methods developed in this paper can become a useful tool for investigation of a number of unsolved problems in optics of colloidal aggregates of noble metals and, more generally, nanosystems consisting of multiple spheres. The possibility to calculate optical responses with the account of high multipole moments for a large number of interacting spheres is needed for more accurate interpretation of experimental data. Account of higher multipoles is especially important in problems where distribution of local field inside the spheres is significant, such as calculation of collective nonlinear effects in aggregated metal colloids. Note that the methods described in this paper can be generalized for calculation of various nonlinear characteristics.

An important material-independent characteristics of optical properties is the density of electromagnetic states (DOS) which studied extensively in this paper for different systems. Note that DOS is closely related to the T matrix of the scattering system and, in the quasistatic limit, is also wavelength independent. The numerical simulations with the account of higher multipoles have revealed that the DOS, for both bispheres and aggregates, approaches its theoretical right bound $w_{\max}=4\pi/3$. As can be seen in Fig. 9, this is not so in the DA. Namely, the DA DOS terminates at approximately $w=2\pi/3$. This fact explains why the pure DA fails to describe accurately the long wavelength properties of most materials. This deficiency of the DA is partially corrected by the GCRM. However, significant discrepancies between the multipole DOS and the GCRM DOS remain, especially near the central peak at $w=0$ (Fig. 13). It is also interesting to note that the DOS calculated in this paper, never extends to its theoretical left bound $w=-8\pi/3$ but terminates at approximately $-4\pi/3$. The DOS at the negative values of w can be important for calculating spectra of high conductivity metals near the plasmon resonance when the spectral variable $X(\omega)$ changes sign and can take large negative values.

The account of higher multipoles for calculation of extinction spectra of random fractal aggregates revealed several features that were not known previously and cannot be understood within the DA or GCRM. First, absorption at the surface plasmon frequency of a single isolated sphere (Frohlich resonance) is much larger than is predicted by the DA or GCRM. The high absorption at the Frohlich frequency was measured experimentally but could not be explained in a self-consistent way; it was attributed earlier to the presence of non-aggregated spheres in the solutions. In this paper we have shown that such explanation is unnecessary. Second, full multipole calculations result in a smaller short-wavelength (below the Frohlich resonance) wing than is predicted by the DA and GCRM, which has been also experimentally observed before.

An important question is convergence of results with the maximum order of included multipoles, L. The maximum value of L that we have used (except for systems with axial symmetry in which extremely large values of L are attainable) were $L=64$ for $N=50$ and $N=100$ and $L=128$ for $N=2$. Results shown in Fig. 5 indicate that these values are sufficient for $\delta \geqslant 0.1$. This includes silver in the near-IR spectral region (with the finite-size corrections for the dielectric function) and black carbon for $\lambda < 100$ μm.

Returning to calculations of extinction spectra, we must emphasize that, ultimately, simulations alone are insufficient to determine the validity of any particular computational method. The model of touching spheres is highly idealized. In practice, the spheres are not perfect and do not touch at a mathematical point. Effects of nonlocality of the dielectric function and polydispersity of the elementary spheres, as well as surface oxidation and coating, can also play an important role, but are very difficult to take into account within a single mathematically tractable model. The approach proposed here is a step toward developing of such a model. However, significant efforts remain to be made. It should be also noted that more phenomenological approaches, such as the GCRM, can be useful when δ is so small that the method developed in this paper fails to converge with L. This is, for example, the case for silver in the far-IR spectral region or for black carbon for $\lambda > 100$ μm.

ACKNOWLEDGMENTS

This research was supported by the Army Research Office through Battelle (Contract No. DAAD19-02-D-0001) and

Presidium of Russian Academy of Sciences ("Basic Problems of Physics and Chemistry of Nanosize Systems and Nanomaterial," Grant 8.1).

APPENDIX: DERIVATION OF THE SUM RULE

The sum rule (20) is a slight generalization of the sum rule previously published for ellipsoids.[82,83] It is obtained by observing that the quantity $\kappa(\omega) \equiv \langle E_0 | P \rangle$ on the right-hand side of Eq. (9) is the so called *generalized susceptibility* as defined in Ref. 84, and must, therefore, satisfy the Kramers-Kronig relations as a function of the electromagnetic frequency ω. In particular

$$\mathrm{Re}[\kappa(\omega)] = \frac{2}{\pi}\int_0^\infty \frac{\omega' \mathrm{Im}[\kappa(\omega')] d\omega'}{\omega'^2 - \omega^2}, \tag{A1}$$

where we have used the symmetry property $\mathrm{Im}[\kappa(-\omega)] = -\mathrm{Im}[\kappa(\omega)]$. By setting $\omega = 0$ in the above formula, we obtain

$$\int_0^\infty \omega^{-1} \mathrm{Im}[\kappa(\omega)] d\omega = \frac{\pi}{2}\mathrm{Re}[\kappa(0)]. \tag{A2}$$

Next we notice that

$$\omega\ \mathrm{Im}\ \kappa(\omega) = \frac{c|\boldsymbol{E}_0|^2}{4\pi}\sigma_e, \tag{A3}$$

which follows directly from Eq. (9). On the other hand, we have

$$\kappa(0) = \boldsymbol{E}_0 \cdot \int \boldsymbol{P}(\boldsymbol{r})|_{\omega=0}\, d^3r = \boldsymbol{E}_0 \cdot \boldsymbol{d}_{\mathrm{tot}}, \tag{A4}$$

where $\boldsymbol{d}_{\mathrm{tot}}$ is the total dipole moment of the scatterer induced by a constant field $\boldsymbol{E}_0$. Define the electrostatic tensor polarizability $\hat{\alpha}$ (which is pure real by definition) and assume that $\boldsymbol{E}_0$ is directed along the z axis. Then

$$\kappa(0) = \alpha_{zz}|\boldsymbol{E}_0|^2, \tag{A5}$$

where α_{zz} is the diagonal element of the tensor $\hat{\alpha}$. Using this result and Eq. (A3), we immediately arrive at

$$\int_0^\infty \omega^{-2}\sigma_e(\omega) d\omega = \frac{2\pi}{c}\alpha_{zz} \tag{A6}$$

or, changing the variable of integration to $\lambda = 2\pi c/\omega$, we obtain Eq. (20). Note that for the rotationally averaged extinction cross section $\langle \sigma_e \rangle$, we also obtain

$$\int_0^\infty \langle \sigma_e(\lambda) \rangle d\lambda = \frac{4\pi^3}{3}\mathrm{Tr}(\hat{\alpha}). \tag{A7}$$

In the earlier derivation we did not use the quasistatic approximation, or the assumption that the dielectric function is scalar and local.

*Author to whom correspondence should be addressed. Electronic address: vmarkel@mail.med.upenn.edu

†Also at: the Institute of Surface Chemistry, National Academy of Sciences of Ukraine, 17 General Naumov St., 03164 Kiev, Ukraine. Electronic address: vitaliy.pustovit@ccaix.jsums.edu

‡Electronic address: karpov@iph.krasn.ru

[1] J. A. Sanchez-Gil, J. V. Garcia-Ramos, and E. R. Mendez, Phys. Rev. B **62**, 10515 (2000).

[2] S. V. Karpov, A. L. Bas'ko, A. K. Popov, and V. V. Slabko, Colloid J. **62**, 699 (2000).

[3] N. G. Khlebtsov, L. A. Dykman, Y. M. Krasnov, and A. G. Mel'nikov, Colloid J. **62**, 765 (2000).

[4] C. M. Sorensen, Aerosol Sci. Technol. **35**, 648 (2001).

[5] H. Kimura, J. Quant. Spectrosc. Radiat. Transf. **70**, 581 (2001).

[6] V. P. Drachev, D. W. Bragg, V. A. Podolsky, V. P. Safonov, W.-T. Kim, Z. C. Ying, R. L. Armstrong, and V. M. Shalaev, J. Opt. Soc. Am. B **18**, 1896 (2001).

[7] W. Wenseleers, F. Stellacci, T. Meyer-Fridrichsen, T. Mangel, C. A. Bauer, S. J. K. Pond, S. R. Marder, and J. W. Perry, J. Phys. Chem. B **106**, 6853 (2002).

[8] S. V. Karpov, A. L. Bas'ko, A. K. Popov, V. V. Slabko, and T. F. George, *Recent Research Developments in Optics* (Research Singpost, Trivandrum, India, 2002), Vol. 2, pp. 427–463.

[9] G. P. Ortiz and W. L. Mochan, Phys. Rev. B **67**, 184204 (2003).

[10] S. V. Karpov, A. L. Bas'ko, A. K. Popov, and V. V. Slabko, Opt. Spectrosc. **95**, 230 (2003).

[11] S. V. Karpov and V. V. Slabko, *Optical and Photophysical Properties of Fractal-Structured Metal Sols* (Russian Academy of Sciences, Siberian Branch, Novosibirsk, 2003).

[12] V. M. Shalaev and M. I. Stockman, Z. Phys. D: At., Mol. Clusters **10**, 71 (1988).

[13] A. V. Butenko, V. M. Shalaev, and M. I. Stockman, Z. Phys. D: At., Mol. Clusters **10**, 81 (1988).

[14] A. V. Butenko, P. A. Chubakov, Y. E. Danilova, S. V. Karpov, A. K. Popov, S. G. Rautian, V. P. Safonov, V. V. Slabko, V. M. Shalaev, and M. I. Stockman, Z. Phys. D: At., Mol. Clusters **17**, 283 (1990).

[15] M. I. Stockman, L. N. Pandey, L. S. Muratov, and T. F. George, Phys. Rev. Lett. **72**, 2486 (1994).

[16] V. M. Shalaev, R. Botet, D. P. Tsai, J. Kovacs, and M. Moskovits, Physica A **207**, 197 (1994).

[17] V. P. Drachev, S. V. Perminov, S. G. Rautian, and V. P. Safonov, JETP Lett. **68**, 651 (1998).

[18] S. V. Karpov, A. K. Popov, S. G. Rautian, V. P. Safonov, V. V. Slabko, V. M. Shalaev, and M. I. Shtokman, JETP Lett. **48**, 571 (1988).

[19] T. T. Rantala, M. I. Stockman, and T. F. George, in *Scaling in Disordered Materials: Fractal Structure and Dymnamics*, edited by T. A. Witten, M. O. Robbins, and J. P. Stokes (Materials Research Society, Pittsburgh, 1990), pp. 117–120.

[20] Y. E. Danilova, A. I. Plekhanov, and V. P. Safonov, Physica A **185**, 61 (1992).

[21] Y. E. Danilova, S. G. Rautian, and V. P. Safonov, Bull. Russ. Acad. Sci. Phys. **60**, 374 (1996).
[22] V. P. Safonov, V. M. Shalaev, V. Markel, Y. E. Danilova, N. N. Lepeshkin, W. Kim, S. G. Rautian, and R. L. Armstrong, Phys. Rev. Lett. **80**, 1102 (1998).
[23] W. D. Bragg, V. A. Markel, W. Kim, K. Banerjee, M. R. Young, J. G. Zhu, R. L. Armstrong, V. M. Shalaev, Z. C. Ying, Y. E. Danilova, and V. P. Safonov, J. Opt. Soc. Am. B **18**, 698 (2001).
[24] S. V. Karpov, A. K. Popov, and V. V. Slabko, Tech. Phys. **73**, 90 (2003).
[25] V. M. Shalaev, M. Moskovits, A. A. Golubentsev, and S. John, Physica A **191**, 352 (1992).
[26] V. M. Shalaev, R. Botet, and A. V. Butenko, Phys. Rev. B **48**, 6662 (1993).
[27] M. I. Stockman, L. N. Pandey, L. S. Muratov, and T. F. George, Phys. Rev. B **51**, 185 (1995).
[28] M. I. Stockman, L. N. Pandey, and T. F. George, Phys. Rev. B **53**, 2183 (1996).
[29] M. I. Stockman, Phys. Rev. E **56**, 6494 (1997).
[30] M. I. Stockman, S. V. Faleev, and D. J. Bergman, Phys. Rev. Lett. **87**, 167401 (2001).
[31] S. R. Forrest and T. A. Witten, J. Phys. A **12**, L109 (1979).
[32] U. O. Koylu and G. M. Faeth, Combust. Flame **89**, 140 (1992).
[33] U. O. Koylu, G. M. Faeth, T. L. Farias, and M. G. Carvalho, Combust. Flame **100**, 621 (1995).
[34] I. Colbeck, B. Atkinson, and Y. Johar, J. Aerosol Sci. **28**, 715 (1997).
[35] M. I. Stockman, Phys. Rev. Lett. **84**, 1011 (2000).
[36] M. V. Berry and I. C. Percival, Opt. Acta **33**, 577 (1986).
[37] V. A. Markel, L. S. Muratov, M. I. Stockman, and T. F. George, Phys. Rev. B **43**, 8183 (1991).
[38] J. E. Sansonetti and J. K. Furdyna, Phys. Rev. B **22**, 2866 (1980).
[39] Y. E. Danilova and V. P. Safonov, in *Fractal Reviews in Natural and Applied Sciences*, edited by M. M. Novak (Chapman & Hall, London, 1995), pp. 101–112.
[40] J. M. Gerardy and M. Ausloos, Phys. Rev. B **22**, 4950 (1980).
[41] F. Claro, Phys. Rev. B **25**, 7875 (1982).
[42] F. Claro, Phys. Rev. B **25**, 2483 (1982).
[43] F. Claro, Phys. Rev. B **30**, 4989 (1984).
[44] F. Claro, Solid State Commun. **49**, 229 (1984).
[45] R. Rojas and F. Claro, Phys. Rev. B **34**, 3730 (1986).
[46] F. Claro and R. Fuchs, Phys. Rev. B **44**, 4109 (1991).
[47] D. W. Mackowski, J. Opt. Soc. Am. A **11**, 2851 (1994).
[48] D. W. Mackowski, Appl. Opt. **34**, 3535 (1995).
[49] D. W. Mackowski and M. Mishchenko, J. Opt. Soc. Am. A **13**, 2266 (1996).
[50] D. W. Mackowski, J. Quant. Spectrosc. Radiat. Transf. **70**, 441 (2001).
[51] V. A. Markel, V. M. Shalaev, and T. F. George, in *Optics of Nanostructured Materials*, Wiley Series in Lasers and Applications (Wiley-Interscience, New York, 2000), pp. 355–412.
[52] V. A. Markel and V. M. Shalaev, J. Opt. Soc. Am. A **18**, 1112 (2000).
[53] J. E. Martin and A. J. Hurd, J. Appl. Crystallogr. **20**, 61 (1987).
[54] D. J. Bergman, Phys. Rev. B **14**, 4304 (1976).
[55] R. Fuchs and F. Claro, Phys. Rev. B **39**, 3875 (1989).
[56] R. Haydock, *Solid State Physics* (Academic Press, New York, 1980), Vol. 35, pp. 215–294.
[57] Y. E. Danilova, V. A. Markel, and V. P. Safonov, Atmos. Oceanic Opt. **6**, 821 (1993).
[58] V. A. Markel, V. M. Shalaev, E. B. Stechel, W. Kim, and R. L. Armstrong, Phys. Rev. B **53**, 2425 (1996).
[59] S. I. Bozhevolnyi, V. A. Markel, V. Coello, W. Kim, and V. M. Shalaev, Phys. Rev. B **58**, 11 441 (1998).
[60] V. A. Markel, V. M. Shalaev, P. Zhang, W. Huynh, L. Tay, T. L. Haslett, and M. Moskovits, Phys. Rev. B **59**, 10 903 (1999).
[61] S. Corni and J. Tomasi, J. Chem. Phys. **116**, 1156 (2002).
[62] L. Zhao, K. L. Kelly, and G. C. Scahtz, J. Phys. Chem. **107**, 7343 (2003).
[63] L. S. Markel, V. A. Muratov, and M. I. Stockman, Sov. Phys. JETP **71**, 455 (1990).
[64] $\mathcal{H}$ is the Hilbert space of functions that are square integrable in V and have zero divergence at every point in V excluding boundaries. Thus, $\mathcal{H}$ is not identical to $L_2(V)$ but is actually a subspace of the latter.
[65] Note that this definition is slightly different from the one adopted in Ref. 37 and subsequently used in several papers. Namely, in Ref. 37 $z=-X-i\delta$; in addition, $\chi=1/z$ is defined in Ref. 37 as the quasistatic polarizability of a single isolated sphere and has, therefore, dimensionality of length cubed. The quantity χ used in this paper is defined by Eq. (4) and is dimensionless.
[66] C. F. Bohren and D. R. Huffman, *Absorption and Scattering of Light by Small Particles* (Wiley, New York, 1983).
[67] W. C. Chew, *Waves and Fields in Inhomogeneous Media* (Van Nostrand Reinhold, New York, 1990).
[68] P. Meakin, Phys. Rev. Lett. **51**, 1119 (1983).
[69] R. Jullien, M. Kolb, and R. Botet, J. Phys. (Paris), Lett. **45**, L211 (1984).
[70] R. Ruppin, J. Phys. Soc. Jpn. **58**, 1446 (1989).
[71] I. E. Mazets, Tech. Phys. **45**, 8 (2000).
[72] J. A. Soules, Am. J. Phys. **58**, 1195 (1990).
[73] A. V. Paley, A. V. Radchik, and G. B. Smith, J. Appl. Phys. **73**, 3446 (1993).
[74] The expression below contains an additional overall factor of $1/4\pi$ which is necessary to preserve normalization of $\Gamma(w)$.
[75] B. T. Draine, Astrophys. J. **333**, 848 (1988).
[76] V. A. Markel, J. Mod. Opt. **40**, 2281 (1993).
[77] M. A. Ordal, L. L. Long, R. J. Bell, S. E. Bell, R. R. Bell, R. W. Alexander, and C. A. Ward, Appl. Opt. **22**, 1099 (1983).
[78] M. A. Ordal, R. J. Bell, L. L. Alexander, R. W. Long, and M. A. Querry, Appl. Opt. **24**, 4493 (1985).
[79] C. W. Bruce, T. F. Stromberg, K. P. Gurton, and J. B. Mozer, Appl. Opt. **30**, 1537 (1991).
[80] W. H. Dalzell and A. F. Sarofim, J. Heat Transfer **91**, 100 (1969).
[81] P. B. Johnson and R. W. Christy, Phys. Rev. B **6**, 4370 (1972).
[82] E. M. Purcell, Astrophys. J. **158**, 433 (1969).
[83] R. Lai and A. J. Sievers, J. Opt. Soc. Am. A **13**, 1036 (1996).
[84] L. D. Landau, E. M. Lifshitz, and L. P. Pitaevskii, *Statistical Physics*, Course of Theoretical Physics 3rd ed., Vol. 1 (Butterworth-Heinemann, Oxford, 1999).